The Company of **Biologists**

RESEARCH ARTICLE

Kindlin-2 promotes rear focal adhesion disassembly and directional persistence during cell migration

Jie Liu[1],*, Zhongzhen Liu[1],*, Keng Chen[1],*, Wei Chen[1], Xiyuan Fang[1], Meng Li[1], Xuening Zhou[1], Ning Ding[1], Huan Lei[1], Chen Guo[1], Tao Qian[1], Yilin Wang[2], Lin Liu[3], Yonglong Chen[1], Hui Zhao[4], Ying Sun[1,‡], Yi Deng[1,‡] and Chuanyue Wu[5,‡]

ABSTRACT

Cell migration involves front-to-rear asymmetric focal adhesion (FA) dynamics, which facilitates trailing edge detachment and directional persistence. Here, we show that kindlin-2 is crucial for FA sliding and disassembly in migrating cells. Loss of kindlin-2 markedly reduced FA number and selectively impaired rear FA sliding and disassembly, resulting in defective rear retraction and reduced directional persistence during cell migration. Kindlin-2-deficient cells failed to develop serum-induced actomyosin-dependent tension at FAs. At the molecular level, kindlin-2 directly interacted with myosin light chain kinase (MYLK, hereafter referred to as MLCK), which was enhanced in response to serum stimulation. Serum deprivation inhibited rear FA disassembly, which was released in response to serum stimulation. Overexpression of the MLCK-binding kindlin-2 F0F1 fragment (amino acid residues 1–167), which inhibits the interaction of endogenous kindlin-2 with MLCK, phenocopied kindlin-2 deficiency-induced migration defects. Inhibition of MLCK, like loss of kindlin-2, also impaired trailing-edge detachment, rear FA disassembly and directional persistence. These results suggest a role of kindlin-2 in promoting actomyosin contractility at FAs, leading to increased rear FA sliding and disassembly, and directional persistence during cell migration.

KEY WORDS: Actomyosin contraction, Cell migration, Focal adhesion disassembly, Kindlin-2, Rear retraction

INTRODUCTION

Cell migration is an important process whose alteration is intimately associated with many human diseases (Avraamides et al., 2008; Etienne-Manneville, 2008; Mierke et al., 2008; Northey et al., 2017). Cell migratory behavior can be characterized by two independent quantities: linear cell locomotion speed and directional persistence (Lauffenburger and Horwitz, 1996). For efficient directional migration, migrating cells require establishment and maintenance of front-rear polarity (Horwitz and Parsons, 1999; Horwitz and Webb, 2003; Petrie

et al., 2009). When undergoing morphological changes with front protrusions and rear retraction that involve dynamic actin cytoskeleton and actomyosin contraction, cells crawl in the intrinsic front-rear direction (Lauffenburger and Horwitz, 1996; Ridley et al., 2003; Bretscher, 2008; Insall and Machesky, 2009). At the leading edge, actin filament polymerization leads to protrusions, where adhesion to extracellular matrix (ECM) triggers the formation of cell-ECM adhesions (Hynes, 2002; Huttenlocher and Horwitz, 2011). These adhesions establish a link between ECM and the actin cytoskeleton and exert traction forces on the substratum, resulting in generation of net propulsive forces to drive forward cell movement (Ridley et al., 2003; Huttenlocher and Horwitz, 2011; Swaminathan and Waterman, 2016). Adhesions in distinct regions of the cell exhibit asymmetric dynamics during cell migration (Rid et al., 2005; Broussard et al., 2008; Mohl et al., 2012). In the front, the newly formed adhesions undergo turnover during active protrusions, or grow into focal adhesions (FAs) that reinforce cell-ECM adhesion (Dubash et al., 2009; Parsons et al., 2010). At the rear, FA sliding and disassembly are crucial for adhesive release, promoting trailing edge detachment and directional migration (Kirfel et al., 2004; Cramer, 2013; Chi et al., 2014). Actomyosin contractility appears to be a dominant force driving rear retraction when large forces are required (Cramer, 2013). Furthermore, myosin II plays an essential role in establishing migratory front-rear polarity and promoting rear retraction during cell migration (Vicente-Manzanares et al., 2007, 2008, 2011; Wilson et al., 2010).

FA is composed of integrins and a plethora of intracellular proteins (Dubash et al., 2009; Kanchanawong et al., 2010; Horton et al., 2015). Pulling forces generated by actomyosin contraction are required for FA assembly through mechanosensitive protein complexes (Gallant et al., 2005; Oakes and Gardel, 2014; Burridge and Guilluy, 2016). Compared to FA assembly, FA disassembly, however, is less well understood. Various mechanisms have been implicated in FA disassembly, including those involving actomyosin contractility (Broussard et al., 2008). Our understanding of proteins that control front-rear asymmetric FA dynamics during cell migration and their signaling mechanisms, however, remains incomplete.

Kindlins are a family of evolutionarily conserved proteins crucial for integrin-mediated cell-ECM adhesion and signaling (Tu et al., 2003; Montanez et al., 2008; Sun et al., 2019; Chronopoulos et al., 2020; Harburger et al., 2009; Huet-Calderwood et al., 2014). Mammalian kindlin family consists of three members, namely kindlin-1, -2 and -3 (officially known as FERMT1, FERMT2 and FERMT3, respectively). Kindlin-2 is expressed in a broad spectrum of cell types, whereas the expression of kindlin-1 and -3 is more restricted (Larjava et al., 2008; Plow et al., 2009; Rognoni et al., 2016). Genetic knockout (KO) and knockdown studies have shown that kindlin-2 is essential for embryonic development as well as homeostasis and functions of different types of tissue and organ (Sun et al., 2017; Rognoni et al., 2016; Zhang et al., 2016; Pluskota et al., 2011). At the cellular level, kindlin-2 has been implicated in regulation of actin cytoskeleton, cell spreading and

[1]Department of Biology, Guangdong Provincial Key Laboratory of Cell Microenvironment and Disease Research, and Shenzhen Key Laboratory of Cell Microenvironment, Southern University of Science and Technology, Shenzhen 518055, China. [2]Core Research Facilities, Southern University of Science and Technology, Shenzhen 518055, China. [3]Department of Cell Biology and Genetics, College of Life Sciences, Nan Kai University, Tianjin, 300071, China. [4]School of Biomedical Sciences, Faculty of Medicine, The Chinese University of Hong Kong, Hong Kong. [5]Department of Pathology, University of Pittsburgh School of Medicine, Pittsburgh, PA 15261, USA.
*These authors contributed equally to this work

‡Authors for correspondence (dengy@sustech.edu.cn; carywu@pitt.edu; suny@sustech.edu.cn)

Y.S., 0000-0001-6706-5720; Y.D., 0000-0003-1378-015X; C.W., 0000-0003-2536-4014

migration (Shi et al., 2007; Theodosiou et al., 2016; Bottcher et al., 2017; Tu et al., 2003; Yasuda-Yamahara et al., 2018; Bledzka et al., 2016). However, how kindlin-2 functions in cell migration is not completely understood. In this study, we have investigated the function of kindlin-2 in cell migration as well as the underlying mechanism.

RESULTS

Kindlin-2 is crucial for regulation of cell shape and FA dynamics

Cell migration involves coordinated changes of cell shape (Broussard et al., 2008; Oakes and Gardel, 2014). To begin to investigate the functions of kindlin-2 in cell migration, we assessed the effects of

kindlin-2 and/or kindlin-1 deficiency on cell shape modulation. Using CRISPR/Cas9-mediated targeted-gene disruption (Fig. S1A), we knocked out kindlin-2 from human HT1080 cells (Fig. 1A, lane 3) and examined the effect on cell morphology (Fig. 1B). In parallel experiments, either kindlin-1 (Fig. 1A, lane 2), which was also expressed in HT1080 cells or both kindlin-1 and 2 (Fig. 1A, lane 4) were knocked out. On either fibronectin (FN) or collagen IV, kindlin-2 KO cells spread poorly, showing fewer and smaller lamellipodia and a highly elongated morphology compared to that of wild-type HT1080 cells (Figs 1B and 2A), suggesting that kindlin-2 is crucial for HT1080 cell shape modulation. No significant morphological and cell spreading defects were observed in kindlin-1 KO cells (Fig. 1B).
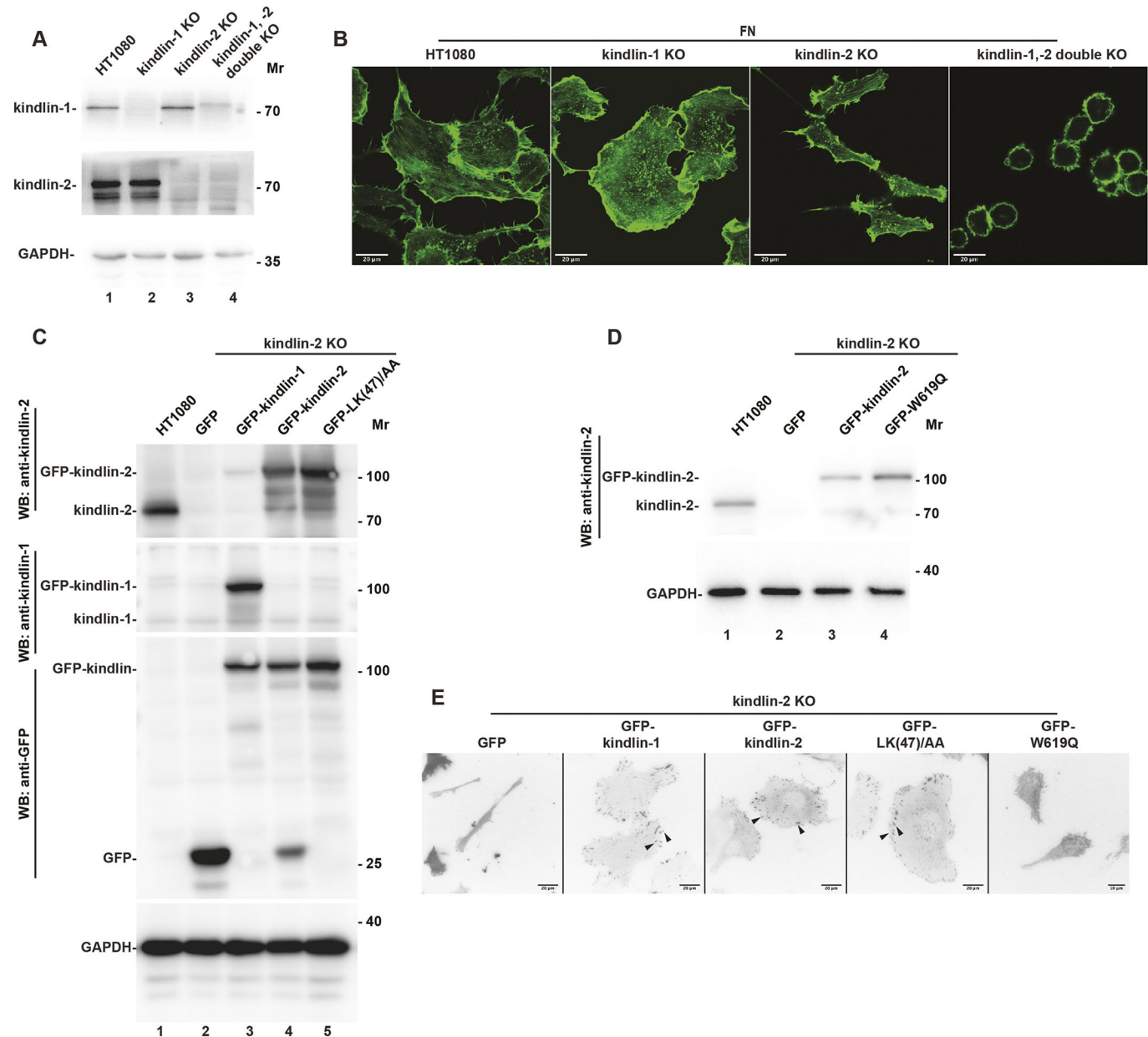
Fig. 1. Loss of kindlin-2 but not kindlin-1 impairs HT1080 cell spreading. (A,C,D) HT1080 wild-type, kindlin-1, -2, and kindlin-1 and -2 double KO cells were analyzed by western blotting as indicated in the figure. Kindlin-1 and/or-2 were depleted in the corresponding KO cells. (B) Morphological changes of kindlin-1, -2, or kindlin-1 and -2 double KO cells. Cells plated on fibronectin (FN) (5 µg/ml) overnight were stained for actin with Alexa 488-conjugated phalloidin. Note that kindlin-2 KO and kindlin-1 and -2 double KO, but not kindlin-1 KO cells, showed dramatic morphological changes. (E) Cells (as indicated) were observed using TIRF microscopy. Note that GFP-kindlin-2, -1, and -LK(47)/AA but not GFP-W619Q mutant kindlin-2 localized to FAs (arrowheads). Scale bars: 20 µm (B, left-hand panels in E) or 10 µm (E, GFP-W619Q panel).
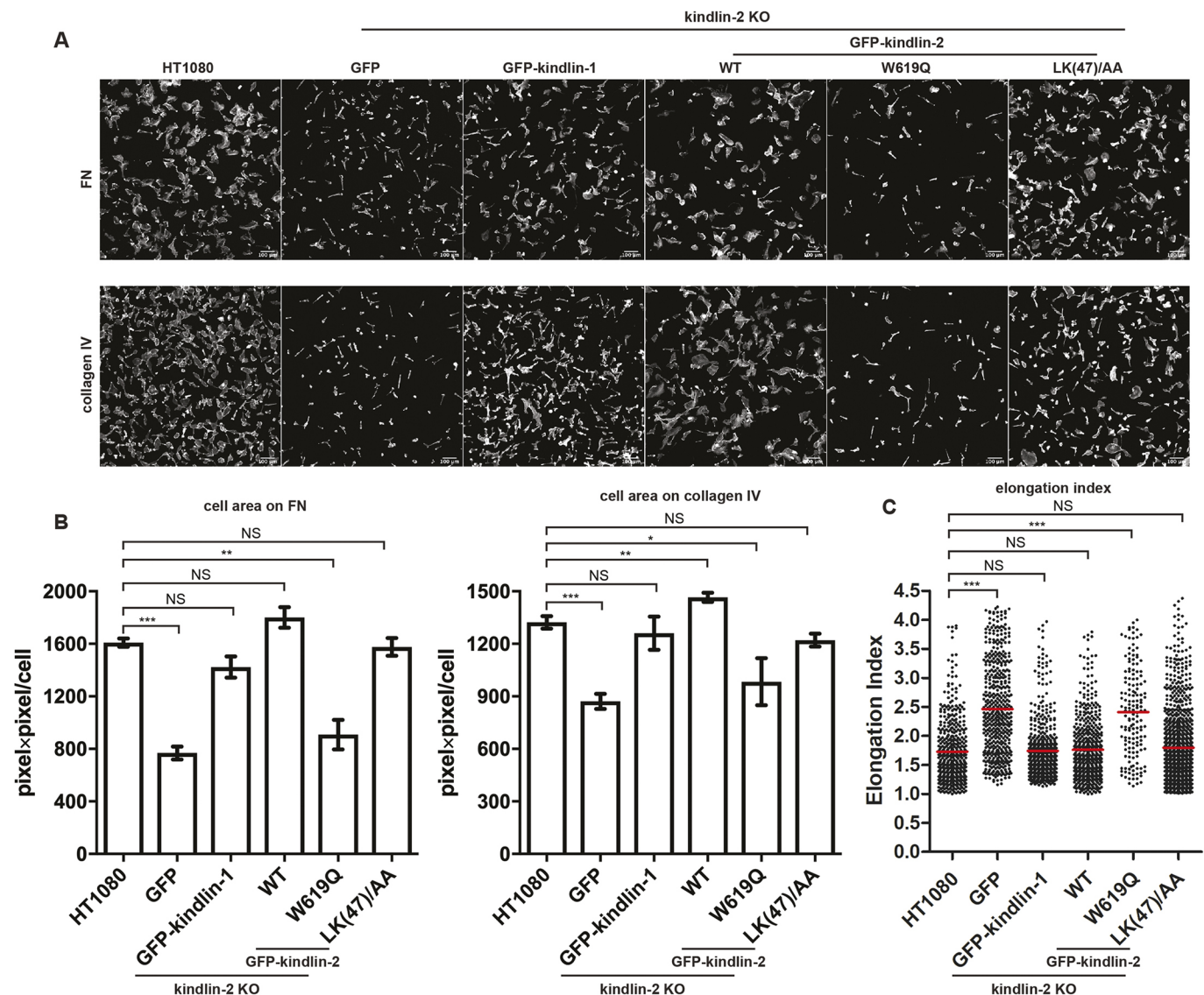
Fig. 2. Quantification of kindlin-2 deficiency-induced morphological changes. (A) Cells as indicated were plated on fibronectin (FN) (5 μg/ml) or collagen IV (5 μg/ml) and stained for actin with Alexa 647-conjugated phalloidin. Scale bars: 100 μm. Expression of GFP-kindlin-1, wild-type (WT) or mutant LK(47)/AA GFP-kindlin-2, but not mutant W619 GFP-kindlin-2, in kindlin-2 KO cells restored cell morphology. (B) Quantification of cell spreading. Data are shown as mean±s.e.m. of pixel×pixel/cell area measured in 4–6 randomly selected fields. *$P<0.05$, **$P<0.005$, ***$P<0.001$. (C) The elongation index, i.e. the length-to-width ratio of cells spreading on FN [$n=454$, 489, 577, 502, 939 and 156 for HT1080 and kindlin-2 KO cells expressing GFP, GFP-kindlin-1, GFP-kindlin-2 WT, GFP-LK(47)/AA and GFP-W619Q, respectively]. The mean is plotted in red. ***$P<0.0001$. NS: not significant.

Regarding kindlin-1 and -2 double KO cells, many of them failed to attach to FN even after prolonged incubation (e.g. overnight); however, those that did attach failed to spread and exhibited a rounded morphology (Fig. 1B). This suggests that the limited spreading observed in the kindlin-2 KO cells was probably supported by the remaining kindlin protein (i.e. kindlin-1) in kindlin-2 KO cells. To further test this, we re-expressed GFP-tagged kindlin-2 and -1, and GFP alone as a control in kindlin-2 KO cells. Western blotting showed that similar levels of GFP-tagged kindlin-2 and -1 were expressed in the corresponding cells (Fig. 1C, compare lanes 3 and 4). Analyses of cell spreading revealed that re-expression of GFP-kindlin-1, like that of GFP-kindlin-2 but not GFP alone, in kindlin-2 KO cells, restored normal cell morphology (Fig. 1E) and spreading (Fig. 2A,B). Thus, when expressed at a level similar to GFP-kindlin-2, GFP-kindlin-1 can functionally substitute GFP-kindlin-2 in promoting cell spreading.

Tryptophan (W) residue 619 in the kindlin-2 F3 domain, and residues leucine (L) 46 as well as lysine (K) 47 (hereafter referred to as LK47) in the F0 domain are crucial for binding to integrin (Li et al., 2017) and actin (Bledzka et al., 2016), respectively. To assess the role of integrin- and actin-binding in kindlin-2-mediated cell shape modulation we, respectively, expressed a GFP-tagged W619Q mutant defective in integrin-binding (Fig. 1D, lane 4), and a GFP-tagged actin-binding-defective mutant LK(47)/AA that comprises an L46A and K47A double substitution to alanine (Fig. 1C, lane 5), in kindlin-2 KO cells. Consistent with previous studies (Bledzka et al., 2016; Li et al., 2017), mutant LK(47)/AA but not W619Q localized to FAs (Fig. 1E). Furthermore, expression of W619Q, unlike that of wild-type kindlin-2 or LK(47)/AA, failed to restore normal cell morphology (Fig. 1E) and spreading (Fig. 2A,B), suggesting that integrin-binding but not LK47-mediated actin-binding is required for kindlin-2-mediated cell spreading.

Kindlin-2 KO cells exhibited a highly elongated morphology on either FN or collagen IV compared to wild-type cells (Fig. 2A). Quantification of the elongation index (i.e. the ratio of length to width of the cell) confirmed that kindlin-2-deficient cells were significantly elongated compared to wild-type cells (Fig. 2C). Re-expression of kindlin-1, wild-type kindlin-2 or LK(47)/AA but not W619Q in kindlin-2 KO cells restored the normal elongation index (Fig. 2C), confirming an essential role of integrin-binding in this process.

Consistent with the elongated cell shape, kindlin-2 KO cells showed smaller leading lamellipodia and drastically stretched trailing tails (Fig. 3A). A 4-fold decrease in the number of FAs per cell was observed in kindlin-2-deficient cells (Fig. 3B), which is consistent with the fact that kindlin-2 is crucial to integrin activation and cell-ECM adhesion (Ma et al., 2008; Harburger et al., 2009). Human HT1080 fibroblasts express multiple integrins including integrins α2, αV, β1 and β3 (Grenz et al., 1993). Consistent with a role of kindlins in the regulation of cell surface integrin levels (Harburger et al., 2009; Margadant et al., 2013, 2012; Kruger et al., 2008; Qu et al., 2011; Schmidt et al., 2011), flow cytometry analyses showed reduced cell surface levels of αVβ3 integrin but modestly increased levels of α2 and β1 integrins in response to loss of kindlin-2 (Fig. S1B). Furthermore, immunofluorescence staining showed clusters of β1 and αVβ3

integrins within many of the remaining FAs in kindlin-2 KO cells, although the level of αVβ3 integrin in some FAs appeared to be reduced (Fig. S1C,D).

It is worth noting that remaining FAs in kindlin-2 KO cells were large and peripheral rather than central FAs (Fig. 3A). In particular, the percentage of large (>15 μm^2) FAs in kindlin-2 KO cells was much higher (∼14%) than that in wild-type cells (∼5%; Fig. 3C). Furthermore, ∼50% of the large FAs were >20 μm^2, and primarily present at the cell edge (Fig. 3A, arrowhead). By contrast, FAs of medium size (2–8 μm^2) were decreased to 44% in kindlin-2 KO cells compared to 57% in wild-type cells (Fig. 3C). Collectively, these results suggest that kindlin-2 play a role in the regulation of FA dynamics.

Kindlin-2 regulates rear retraction and directional persistence in migrating cells

We next investigated the effect of kindlin-2 deficiency on cell migration by using time-lapse imaging. Kindlin-2 KO cells initially spread well on FN, suggesting no obvious initial spreading defect. Approximately 20–25 min after adhering to FN, both wild-type and kindlin-2 KO cells displayed front-back polarity (Fig. 4A,C and Movies 1,2). However, kindlin-2 KO cells assumed the elongated morphology (Fig. 4A and Movie 1). Moreover, whereas wild-type
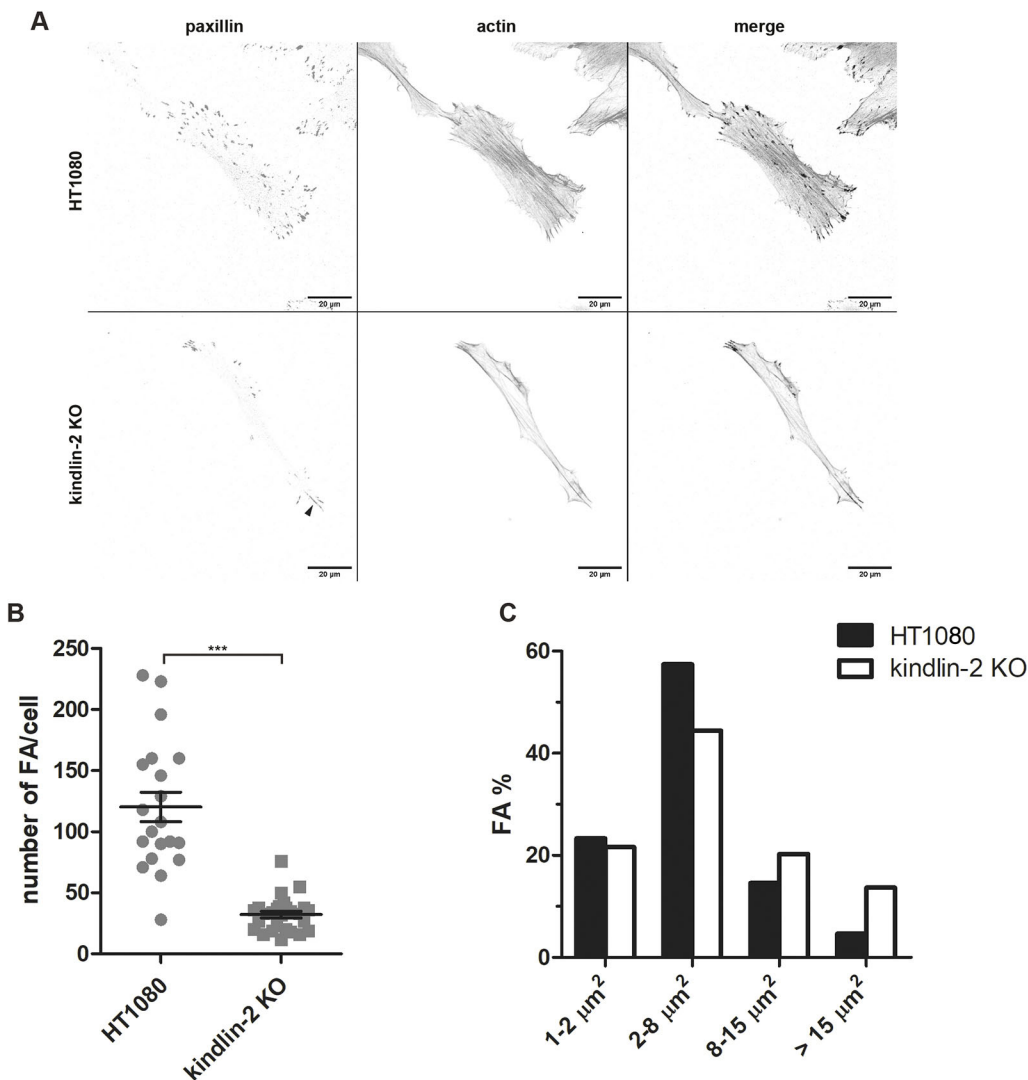
Fig. 3. Loss of kindlin-2 alters FAs. (A) FAs stained with anti-paxillin antibody in HT1080 wild-type or kindlin-2 KO cells. Actin was stained with Alexa 555-conjugated phalloidin. Scale bars: 20 μm. A large FA in kindlin-2 KO cells is indicated by an arrowhead. (B) Quantification of FA density. The mean±s.e.m. is plotted (HT1080: n=20, 120±12 FAs per cell, and kindlin-2 KO: n=27, 32±3 FAs per cell). The number of FAs was significantly reduced in kindlin-2 KO cells. ***P<0.0001. (C) The size of each FA (in μm^2) in HT1080 wild-type (n=2406 FAs) and kindlin-2 KO (n=869 FAs) cells was quantified, and the size distribution of FAs (in %) plotted. Note that the percentage of large (>15 μm^2) FAs was increased in kindlin-2 KO cells.
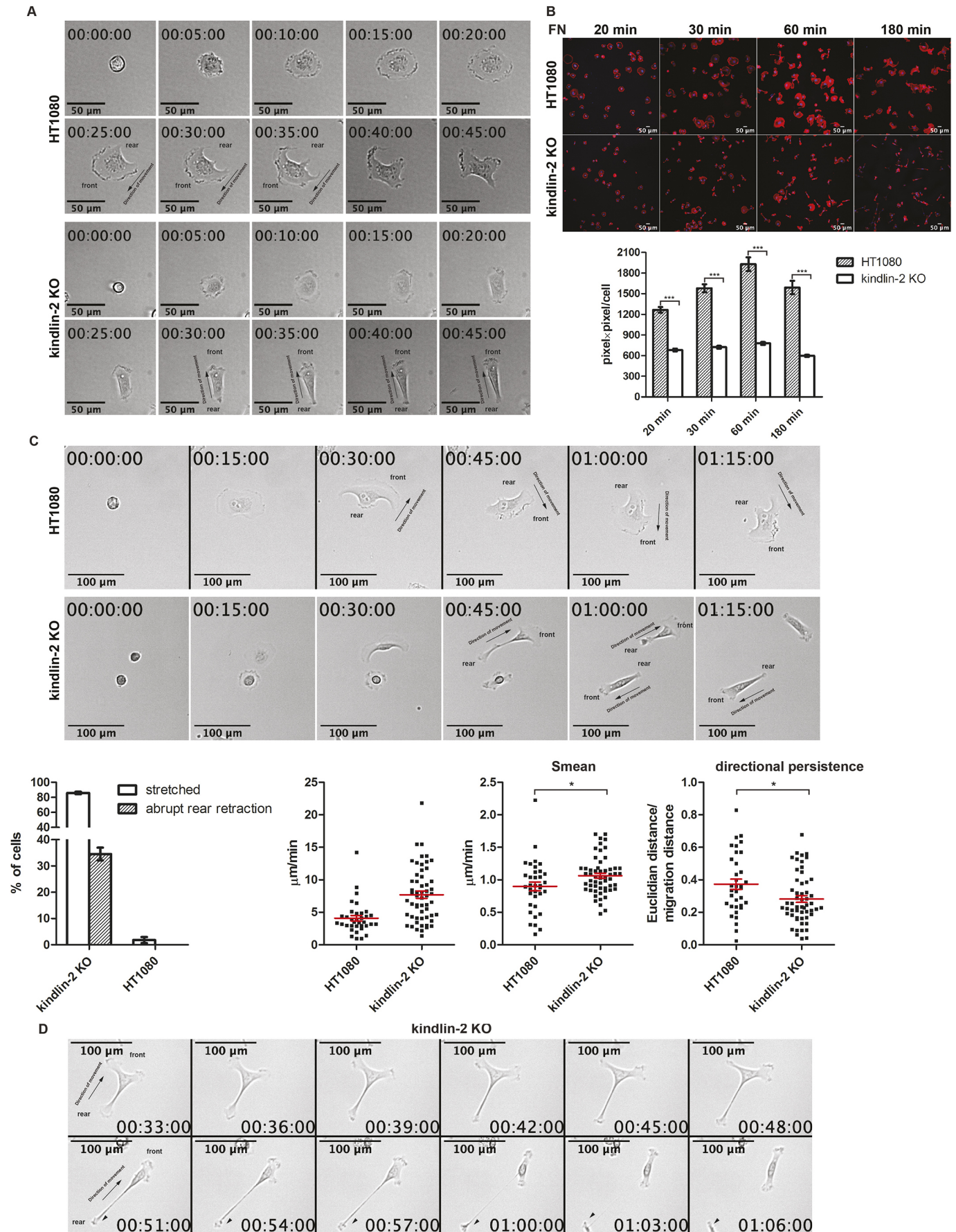
Fig. 4. See next page for legend.

Fig. 4. Loss of kindlin-2 impairs rear retraction and directional persistence in migrating cells. (A) Time-lapse live-cell images of HT1080 wild-type or kindlin-2 KO cells spreading on FN (5 μg/ml) (see Movie 1). (B) Cells as in A plated on FN for the indicated time were fixed and stained with Alexa 555-conjugated phalloidin (actin) and Hoechst dye 33342 (nuclei). Bar graph shows quantification of cell spreading areas. Data are shown as mean±s.e.m. of cell areas measured in 5–9 randomly selected fields. Kindlin-2 KO cells showed reduced cell spreading area. ***$P<0.001$. (C) Time-lapse live-cell images of cell migration (see Movie 2). The percentage of migrating cells being stretched and exhibiting abrupt rear retraction were counted, respectively, in HT1080 ($n=287$) and kindlin-2 KO ($n=312$) cells. Kindlin-2 KO cells exhibited impaired rear retraction. Mean and maximum migration speed (S_{mean} and S_{max}, respectively), and directional persistence were measured. The mean±s.e.m. is plotted in red (HT1080: $n=35$, kindlin-2 KO: $n=56$). S_{mean} and S_{max} were increased, whereas directional persistence was decreased in kindlin-2 KO cells. *$P<0.05$, ***$P<0.0001$. (D) Time-lapse live-cell images showing impaired trailing-edge detachment (arrowhead) of kindlin-2 KO cells during migration (see Movie 3). Scale bars: 50 μm (A,B) or 100 μm (C,D).

cells migrated efficiently, showing lamellipodia formation at the front and trailing edge retraction at the rear, the majority (86%) of kindlin-2 KO cells were stretched, with ~35% of them exhibiting abrupt rear-edge detachment (Fig. 4C, Movie 2). Some kindlin-2 KO cells moved forwards without detachment of the trailing edge, leaving behind a piece of cell body (Fig. 4D, arrowhead, Movie 3). Kindlin-2 deficiency-induced impairment of trailing edge detachment was observed in kindlin-2 KO HT1080 cells seeded on both soft and stiff matrices (Movies 4,5) as well as in other cell types, including human podocytes (Movie 6) and A549 lung adenocarcinoma cells (Movie 7), in which kindlin-2 had been knocked down or depleted (Fig. S2). Cell motility analysis revealed that both mean and maximum migration speed (S_{mean} and S_{max}, respectively) were significantly increased in kindlin-2 KO cells (Fig. 4C, Fig. S2). Notably, directional persistence was significantly reduced in kindlin-2 KO cells (Fig. 4C, Fig. S2). Taken together, these results suggest that kindlin-2 is crucial for trailing edge detachment and directional persistence in migrating cells.

To further test this, we analyzed the migration of kindlin-2 KO cells re-expressing kindlin-1, kindlin-2, W619Q or LK(47)/AA all tagged to GFP (Fig. 1C–D), finding that kindlin-1, kindlin-2 and LK(47)/AA but not W619Q successfully restored rear retraction and coordinated migration in kindlin-2-deficient cells (Fig. S3, Movie 8). Collectively, these data identify an important role of kindlin-2 and kindlin-1 – when expressed at appropriate levels – in promoting rear retraction during cell migration and suggest that this regulation is dependent on kindlin-2 interaction with integrin.

## Kindlin-2 depletion impairs rear FA sliding and disassembly
Rear retraction is coupled to FA disassembly at the cell rear (Broussard et al., 2008). Thus, we analyzed the effect of kindlin-2 deficiency on FA dynamics by using time-lapse TIRF microscopy. Paxillin, a marker of FAs, tagged to Ruby2 was manually tracked, and FAs dynamics at the cell front and rear were analyzed (Fig. 5A) (Stehbens and Wittmann, 2014). Concurrent with rear retraction, FAs at the cell rear slid and were rapidly ripped off by rear retraction in wild-type cells (Movie 9). The disassembly rate (K_d) of rear FAs was approximately twice as high as that of frontal ones (Fig. 5B), whereas the FA assembly rate (K_a) in the front was similar to that at the rear (Fig. 5B). Thus, there is a front-rear polarization in terms of FA disassembly in wild-type cells. By contrast, FAs at the rear barely slid and appeared rather stable in kindlin-2 KO cells, preventing the rear edge from retraction (Movie 9). Here, the K_d was significantly decreased compared to that in wild-type cells, whereas the K_d of FAs in the front was not changed significantly (Fig. 5B).

Thus, unlike wild-type cells, in which FAs at the rear disassembled faster than those at the front, kindlin-2 KO cells exhibited indistinguishable K_d values of front and rear FAs, suggesting that loss of kindlin-2 impairs the front-rear polarization of FA disassembly. We also tracked FA dynamics in the front and rear of kindlin-2 KO HT1080 cells that re-expressed GFP-tagged kindlin-1, kindlin-2 or LK(47)/AA by using GFP-tagged kindlin proteins as markers for FAs. Similar to wild-type HT1080 cells (Fig. 5A) – and consistent with the ability of kindlin-1, kindlin-2 or -LK(47)/AA to restore rear retraction and coordinated migration in kindlin-2 KO cells (Fig. S3, Movie 8) – these cells exhibited similar front-rear polarization of FA dynamics (i.e. faster FA disassembly at the cell rear) (Fig. 5C,D, Movie 10). This indicates that (1) kindlin-1 is functionally similar to kindlin-2 in this process when expressed at an appropriate level and (2) LK47-mediated actin-binding is not essential for establishment of this front-rear polarization of FA dynamics.

Kindlin-2 depletion impairs serum-induced regulation of actomyosin contractility
Because cellular contractile machinery has been implicated in FA disassembly and trailing edge detachment during cell migration (Ridley et al., 2003; Gupton and Waterman-Storer, 2006; Parsons et al., 2010), we sought to test whether loss of kindlin-2 affects actomyosin contractility at FAs. To do this, we employed TLN HP35, a FRET-based talin tension sensor that responds to actomyosin-dependent mechanical force at FAs (Austen et al., 2015). As it is known that serum stimulates stress fiber formation in serum-deprived cells, leading to increased actomyosin-dependent tension (Burridge and Guilluy, 2016), we tested whether kindlin-2 is required for serum-induced actomyosin contractility at FAs. Five minutes after serum stimulation, concurrent with stress fiber formation (Fig. 6A), a significant increase in the fluorescence lifetime of TLN HP35 ($\tau_{\text{TLN HP35}}=2.48\pm0.120$ ns, $n=7$) was detected compared to the zero-force control (TLN CTL) ($\tau_{\text{TLN CTL}}=2.07\pm0.025$ ns, $n=10$) (Fig. 6B, Fig. S2). This corresponded to a FRET efficiency of 14.3%, ~50% reduction of FRET efficiency (27.8%) of the zero-force control (Fig. 6B), indicating that actomyosin-dependent tension at FAs developed upon serum stimulation. Fifteen minutes after serum stimulation, fluorescence lifetime of TLN HP35 ($\tau_{\text{TLN HP35}}=2.23\pm0.068$ ns, $n=9$) was slightly decreased (FRET efficiency =22.2%) and remained virtually unchanged for the duration of measurements ($\tau=2.30\pm0.038$ ns, FRET efficiency=19.1%, $n=16$, and $\tau=2.22\pm0.046$ ns, FRET efficiency=22.2%, $n=7$ for 30-min and 60-min serum stimulation, respectively) (Fig. 6B, Fig. S2). Importantly, upon serum stimulation, fluorescence lifetime of TLN HP35 ($\tau_{\text{TLN HP35}}=2.13\pm0.028$ ns, $n=10$) in kindlin-2 KO cells barely changed compared to that of zero-force control ($\tau_{\text{TLN CTL}}=2.12\pm0.041$ ns, $n=9$) essentially showing the same FRET efficiency (28% and 28.3%) for TLN HP35 and TLN CTL, respectively (Fig. 6B, Fig. S4). This suggests that kindlin-2 is crucial for serum-induced actomyosin contraction at FAs.

In the absence of serum stimulation, the fluorescence lifetime of TLN HP35 ($\tau_{\text{TLN HP35}}=2.07\pm0.016$ ns, FRET efficiency=23.4%, $n=12$) in HT1080 cells was only slightly higher than that of the zero-force control TLN CTL ($\tau_{\text{TLN CTL}}=1.95\pm0.012$ ns, FRET efficiency=27.8%, $n=11$) (Fig. 6C), indicating a relatively low basal tension at FAs under this condition. Under the same conditions, in kindlin-2 KO cells the fluorescence lifetime of TLN HP35 ($\tau_{\text{TLN HP35}}=2.10\pm0.022$ ns, FRET efficiency=23.4%, $n=10$) was also only slightly higher than that of the zero-force control TLN CTL ($\tau_{\text{TLN CTL}}=1.94\pm0.015$ ns, FRET
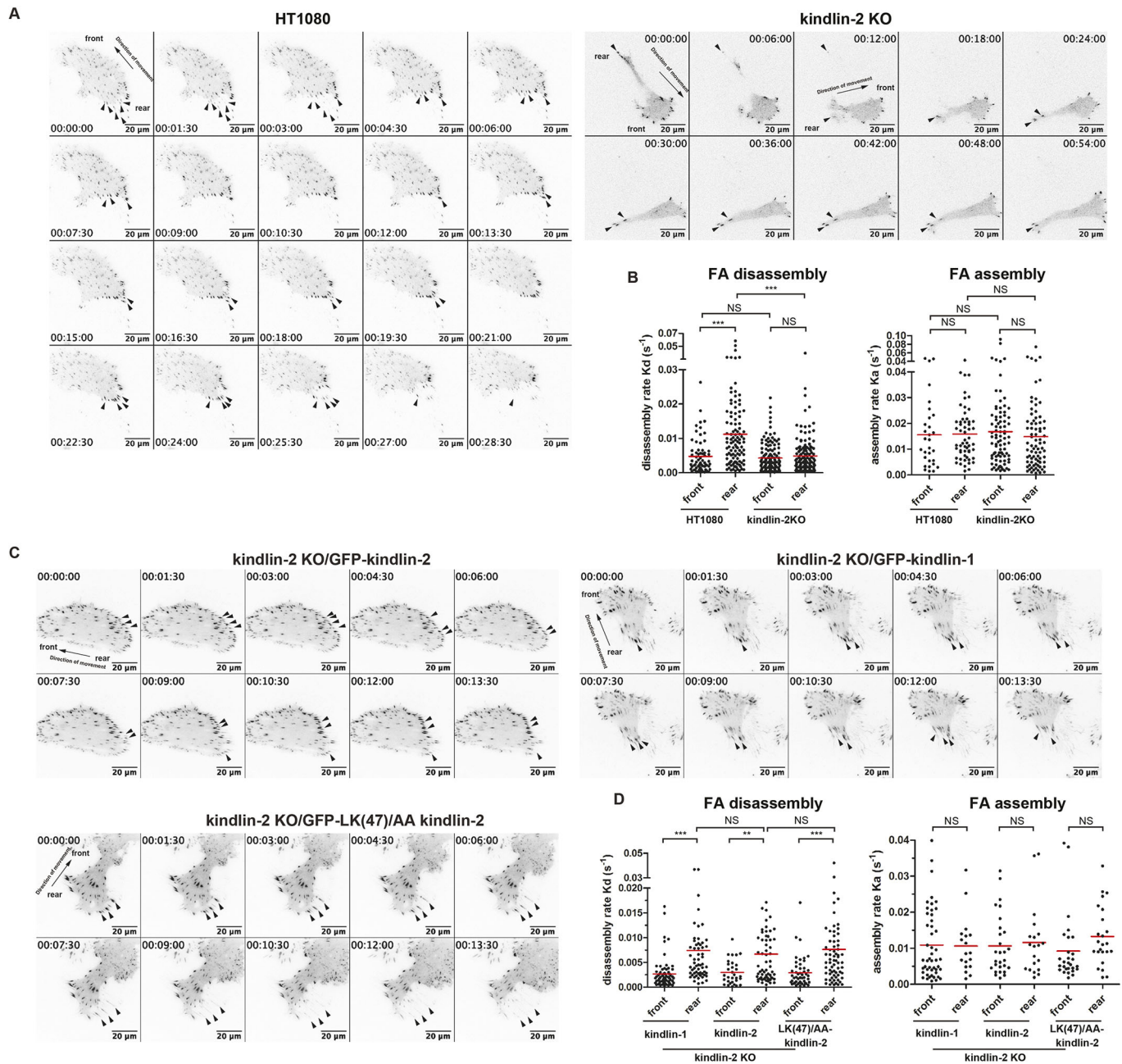
Fig. 5. Loss of kindlin-2 impairs cell rear FA disassembly. (A) Time-lapse TIRF images of paxillin-Ruby2 (arrowheads) stably expressed in HT1080 and kindlin-2 KO cells (see Movie 10). (B) Quantification of FA disassembly (K_d) and assembly (K_a) rates indicated by paxillin-Ruby2 in the front and rear region of migrating cells. The mean is plotted in red. HT1080 cells: at cell front K_d=0.0048±0.0006 s^{-1} (n=67) and K_a=0.0156±0.002 s^{-1} (n=30), at cell rear K_d=0.011 ±0.001 s^{-1} (n=105) and K_a=0.0159±0.001 s^{-1} (n=57). Kindlin-2 KO cells: at cell front K_d=0.0043±0.0003 s^{-1} (n=133) and K_a=0.0168±0.0016 s^{-1} (n=86), at the cell rear K_d=0.0049±0.0004 s^{-1} (n=139) and K_a=0.0149±0.0015 s^{-1} (n=79). Note that K_d was increased at cell rear in HT1080 wild-type but not kindlin-2 KO cells. ***P<0.0001. (C) Time-lapse TIRF images of GFP-kindlin-1, -2 or -LK(47)/AA expressed in kindlin-2 KO cells (arrowheads, see Movie 11). (D) Quantification of K_d and K_a indicated by GFP-kindlin proteins in FAs in the front and rear region of migrating cells. The mean is plotted in red. Kindlin-2 KO/GFP-kindlin-1 cells: at the front K_d=0.0027±0.0003 s^{-1} (n=73) and K_a=0.011±0.0014 s^{-1} (n=48), at the rear K_d=0.0074±0.001 s^{-1} (n=60) and K_a=0.011±0.0018 s^{-1} (n=18). Kindlin-2 KO/GFP-kindlin-2 cells: at the front K_d=0.0030±0.0004 s^{-1} (n=31) and K_a=0.011±0.0016 s^{-1} (n=28), at the rear K_d=0.0066±0.0008 s^{-1} (n=63) and K_a=0.012± 0.0022 s^{-1} (n=20). Kindlin-2 KO/GFP-LK(47)/AA cells: at the front K_d=0.0029±0.0004 s^{-1} (n=49) and K_a=0.0092±0.0018 s^{-1} (n=28), at the rear K_d=0.0076± 0.0009 s^{-1} (n=70) and K_a=0.013±0.0017 s^{-1} (n=24). Re-expression of GFP-kindlin-1, -2, or LK(47)/AA-kindlin-2 in kindlin-2 KO cells restored faster K_d at the cell rear. **P<0.005, ***P<0.001. Scale bars: 20 µm. NS: not significant.

efficiency=29.5%, n=7) (Fig. 6C), suggesting that the relatively low basal tension at FAs was not noticeably affected by the loss of kindlin-2. Thus, although kindin-2 is crucial for serum stimulation-induced tension at FAs, it did not exert a significant effect on basal tension levels at FAs.

We next assessed the effect of serum stimulation on cell migration and FA turnover. After serum deprivation, wild-type cells appeared smaller and elongated (Fig. S5A, Movie 11), reminiscent of the shape of kindlin-2 KO cells (Fig. 1). During cell migration, the trailing edge of wild-type cells was stretched and cell motility was
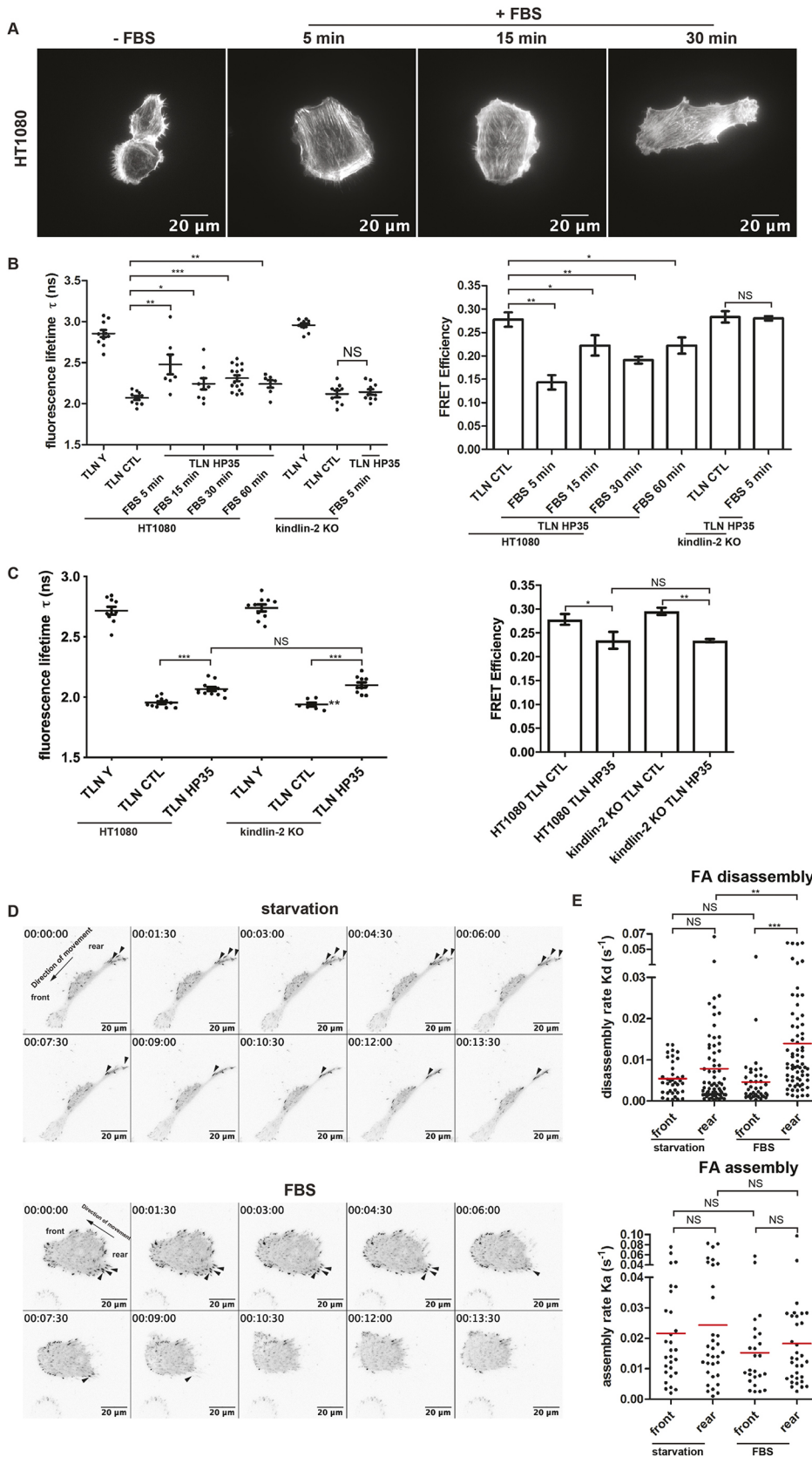
Fig. 6. Kindlin-2 is essential for serum-induced tension at FAs. (A) Confocal fluorescence images of FBS-induced stress fiber formation in serum-starved HT1080 cells. Cells cultured for 24 h in serum-deprived (−FBS) medium were stimulated with 10% FBS for the indicated time and stained for actin with Alexa 488-conjugated phalloidin. Note that actin stress fibers were reinforced in response to serum stimulation. (B) Left: fluorescence lifetime (τ in ns) of TLN Y (donor-only control), zero-force control (TLN CTL) and TLN HP35 in HT1080 or kindlin-2 KO cells upon serum stimulation for different durations as indicated (see Fig. S2). The mean±s.e.m. of τ is plotted. In HT1080 cells, $\tau_{TLN\ Y}$=2.85±0.043 ns (n=10), $\tau_{TLN\ CTL}$=2.07±0.025 ns (n=10), FBS 5 min $\tau_{TLN\ HP35}$=2.48±0.120 ns (n=7), FBS 15 min $\tau_{TLN\ HP35}$=2.23±0.068 ns (n=9), FBS 30 min $\tau_{TLN\ HP35}$=2.30±0.038 ns (n=16), FBS 60 min $\tau_{TLN\ HP35}$=2.22±0.046 ns (n=7). In kindlin-2 KO cells, $\tau_{TLN\ Y}$=2.96±0.023 ns (n=10), $\tau_{TLN\ CTL}$=2.12±0.041 ns (n=9), FBS 5 min $\tau_{TLN\ HP35}$=2.13±0.028 ns (n=10). Note that τ was increased upon serum stimulation in HT1080 wild-type cells but not in kindlin-2 KO cells. *P<0.05, **P<0.01, ***P<0.0001. Right: FRET efficiency was calculated as described in Materials and Methods. Data are shown as mean±s.e.m. *P<0.05, **P<0.01. (C) Left: Fluorescence lifetime (τ in ns) of TLN Y, TLN CTL and TLN HP35 in HT1080 or kindlin-2 KO cells under basal conditions. The mean±s.e.m. of τ is plotted. In HT1080 cells, $\tau_{TLN\ Y}$=2.72±0.032 ns (n=10), $\tau_{TLN\ CTL}$=1.95±0.012 ns (n=11), $\tau_{TLN\ HP35}$=2.07±0.016 ns (n=12). In kindlin-2 KO cells, $\tau_{TLN\ Y}$=2.74±0.030 ns (n=10), $\tau_{TLN\ CTL}$=1.94±0.015 ns (n=7), $\tau_{TLN\ HP35}$=2.10±0.022 ns (n=10). ***P<0.0001. Note that under basal conditions, τ was similar in both HT1080 wild-type and kindlin-2 KO cells. Right: FRET efficiency was calculated as in B. *P<0.05, **P<0.01. (D) Time-lapse TIRF images of HT1080 cells stably expressing paxillin-Ruby2 (arrowheads) under in serum-deprived (for 24 h) or FBS-stimulated conditions (see Movie 14). (E) Quantification of the FA disassembly (K_d) and assembly (K_a) rates in serum-starved and FBS-stimulated migrating cells, respectively. The mean is plotted in red. Serum-starved cells: at cell front K_d=0.0055±0.0006 s^{-1} (n=37) and K_a=0.022±0.003 s^{-1} (n=29), at cell rear K_d=0.078±0.0012 s^{-1} (n=70) and K_a=0.024±0.004 s^{-1} (n=33). Serum-stimulated cells: at cell front K_d=0.0046±0.001 s^{-1} (n=42) and K_a=0.015±0.003 s^{-1} (n=25), at cell rear K_d=0.014±0.0017 s^{-1} (n=68) and K_a=0.018±0.003 s^{-1} (n=33). Note that K_d at the cell rear was increased upon serum stimulation. **P<0.005, ***P<0.0001. Scale bars: 20 μm. NS: not significant.

slow (Movie 11). Notably, serum deprivation markedly reduced FA disassembly at the cell rear (Fig. 6E,F, Movie 13), which was again similar to the phenotypes observed in kindlin-2 KO cells (Fig. 5A, Movie 9). Upon addition of serum to the culture medium, cell motility was increased (Fig. S5B, Movie 11) and serum deprivation-induced inhibition of FA disassembly at the cell rear was released

(Fig. 6D,E, Movie 13), indicating a link between serum stimulation and increased FA disassembly at the cell rear. Kindlin-2 KO cells cultured under serum-deprived conditions were much smaller and even became rounded (Fig. S5A, Movie 12), and formed fewer FAs (data not shown). Serum stimulation promoted the motility of kindlin-2-deficient cells (i.e. Smean and Smax) with decreased directional persistence compared to that of wild-type cells (Fig. S5B, Movie 12), which was consistent with the results obtained under normal resting conditions in the presence of serum (Fig. 4). Taken together, these data indicate that serum stimulation promotes rear FA disassembly and cell migration.

Interaction between kindlin-2 and MLCK regulates MLC phosphorylation and cell migration

We next sought to investigate the molecular mechanism by which kindin-2 functions in serum-induced regulation of actomyosin contraction. We have recently found that kindlin-2 forms a complex with myosin light chain kinase (MYLK, hereafter referred to as MLCK) (Guo et al., 2018), which is known to catalyze myosin regulatory light chain (MYL2, hereafter referred to as MLC) phosphorylation at Ser19 and Thr18 ($pMLC^{Ser19/Thr18}$) (Itoh et al., 1992) and regulate actomyosin contraction (Adelstein, 1982). Consistent with this, MLCK was readily immunoprecipitated together with GFP-kindlin-2 or GFP-kindlin-1, but not with GFP control (Fig. S6). Furthermore, serum stimulation of wild-type HT1080 cells significantly increased the association between kindlin-2 and MLCK (Fig. 7A) and the level of $pMLC^{Ser19/Thr18}$ (Fig. 7B, compare lanes 2 and 1). By marked contrast, no significant increase of $pMLC^{Ser19/Thr18}$ was detected in kindlin-2 KO cells in response to serum stimulation (Fig. 7B, compare lanes 4 and 3), suggesting that kindlin-2 is required for serum-induced phosphorylation of MLC. Furthermore, when seeded on soft matrices, which reportedly downregulates actomyosin contractility (Mih et al., 2012), serum-stimulation-induced MLC phosphorylation was also reduced (Fig. 7C, compare lanes 4 and 3). Together, these observations explain why kindlin-2-deficient cells were incapable to develop actomyosin-dependent tension at FAs in response to serum stimulation (Fig. 6).

Although we have shown previously that kindlin-2 forms a complex with MLCK (Guo et al., 2018), it was not known whether the interaction is direct or indirect. To test this, we expressed and purified glutathione S-transferase (GST)-tagged kindlin-2 together with maltose-binding protein (MBP)-tagged MLCK, and analyzed their interaction. The results showed that GST-kindlin-2 was readily pulled down by MBP-MLCK (Fig. 7D, lane 6) but not MBP (Fig. 7C, lane 5), suggesting that kindlin-2 directly interacts with MLCK.

Next, we sought to map the kindlin-2 domain that mediates MLCK-binding. GST pulldown assay demonstrated that kindlin-2 F0-F1 domains (Fig. 7E, lane 4), like kindlin-2 (Fig. 7E, lane 2), were sufficient to pull down MLCK, whereas F0, F2 or F2-F3 failed to do so (Fig. 7E, lanes 3, 5 and 6), suggesting that F1 is crucial for MLCK-binding. To further test this, we expressed a GFP-tagged kindlin-2 fragment containing amino acid (aa) residues 1–167, i.e. GFP-F0F1 (1–167), which encompasses the F0 and F1 N-terminal regions before the long inserted sequence (aa 168–217) in the F1 lobe (Li et al., 2017) and GFP as a control in HT1080 cells. Co-immunoprecipitation showed that GFP-F0F1 (1–167) but not GFP alone readily bound MLCK (Fig. 7F, compare lanes 4 and 3). Overexpression of GFP-F0F1 (1–167) significantly inhibited the interaction between endogenous kindlin-2 and MLCK (Fig. 7F, compare lane 4 with lane 3) and serum-induced MLC phosphorylation (Fig. 7H, compare lanes 3 and 1). Importantly,

similar to loss of kindlin-2 (Fig. 4C; Fig. S2), overexpression of GFP-F0F1 (1–167) impaired rear retraction, reduced directional persistence and increased the speed of migration (Fig. 7G, Movie 14), although kindlin-2 and paxillin were detected in the retracting rear of these cells (Fig. 7I and J). Collectively, these results suggest that the interaction between kindlin-2 and MLCK is crucial for regulation of cell migration.

Inhibition of MLCK phenocopies kindlin-2 -induced defects in rear FA disassembly and cell migration

The results described above suggest that the interaction between kindlin-2 and MLCK promotes MLC phosphorylation and, consequently, actomyosin contraction, rear FA disassembly and retraction, as well as directional persistence. This implies that inhibition of MLCK results in migration defects similar to those caused by kindlin-2 deficiency. To test this, we treated HT1080 cells with the MLCK inhibitor ML-7 (Webb et al., 2002; Lou et al., 2015). As expected, the level of $pMLC^{Ser19/Thr18}$ was reduced upon ML-7 treatment (Fig. 8A). Compared to control cells, ML-7-treated cells showed decreases and increases in cell spreading area and elongation index, respectively (Fig. 8B), both being reminiscent of kindlin-2-deficient cells (Fig. 2). Furthermore, like kindlin-2-deficient cells (Movie 2), the majority (~90%) of ML-7-treated cells showed stretched trailing tails resulting from impaired trailing edge detachment during migration (Fig. 8C,D, Movies 15,16). Similar to our observation in kindlin-2-deficient cells, Smean and Smax of migration were increased, and the directional persistence was reduced in response to inhibition of MLCK (Fig. 8E). Unlike wild-type HT1080 cells, kindlin-2 KO cells treated with ML-7 showed no changes in Smax and directional persistence, but a slight increase in Smean (Fig. 8E), suggesting that effects of ML-7 on cell migration largely depend on the presence of kindlin-2. Finally, FA disassembly at the cell rear was also significantly decreased in response to MLCK inhibition (Fig. 8F,G, Movie 17). Thus, the migration defects induced by inhibition of MLCK are reminiscent to those caused by loss of kindlin-2, i.e. increased migration speed, impaired rear retraction with slow FA disassembly at the rear and reduced directional persistence, which supports the notion that kindlin-2 functions in regulation of cell migration by – at least in part – facilitating MLCK function.

DISCUSSION

Cell migration is a dynamic and polarized process that requires adhesion at the cell front and adhesion release at the cell rear (Parsons et al., 2010; Cramer, 2013; Ladoux et al., 2016). This process is closely associated with continuous assembly and disassembly of FAs in the leading edge, and periodical sliding and disassembly of FAs at the trailing edge (Ridley et al., 2003; Broussard et al., 2008; Parsons et al., 2010). Siding and disassembly of FAs at the rear allow detachment of trailing edge, resulting in cell translocation and efficient migration. Therefore, the establishment and maintenance of front-rear asymmetric FA disassembly and sliding are crucial for efficient directional cell migration. Substantial evidence indicates that the front-rear polarization is elicited and achieved through regulation of cytoskeleton dynamics and orientation, FAs and the contractile machinery in response to various stimulations (Ladoux et al., 2016). However, the proteins that regulate this process are not yet completely understood. Non-muscle myosin II plays an essential role in establishing migratory front-rear polarity in mammalian cells and promoting rear retraction during cell migration (Vicente-Manzanares et al., 2007, 2008, 2011; Wilson et al., 2010). In this current study, we demonstrated that kindlin-2 – a broadly expressed and evolutionarily
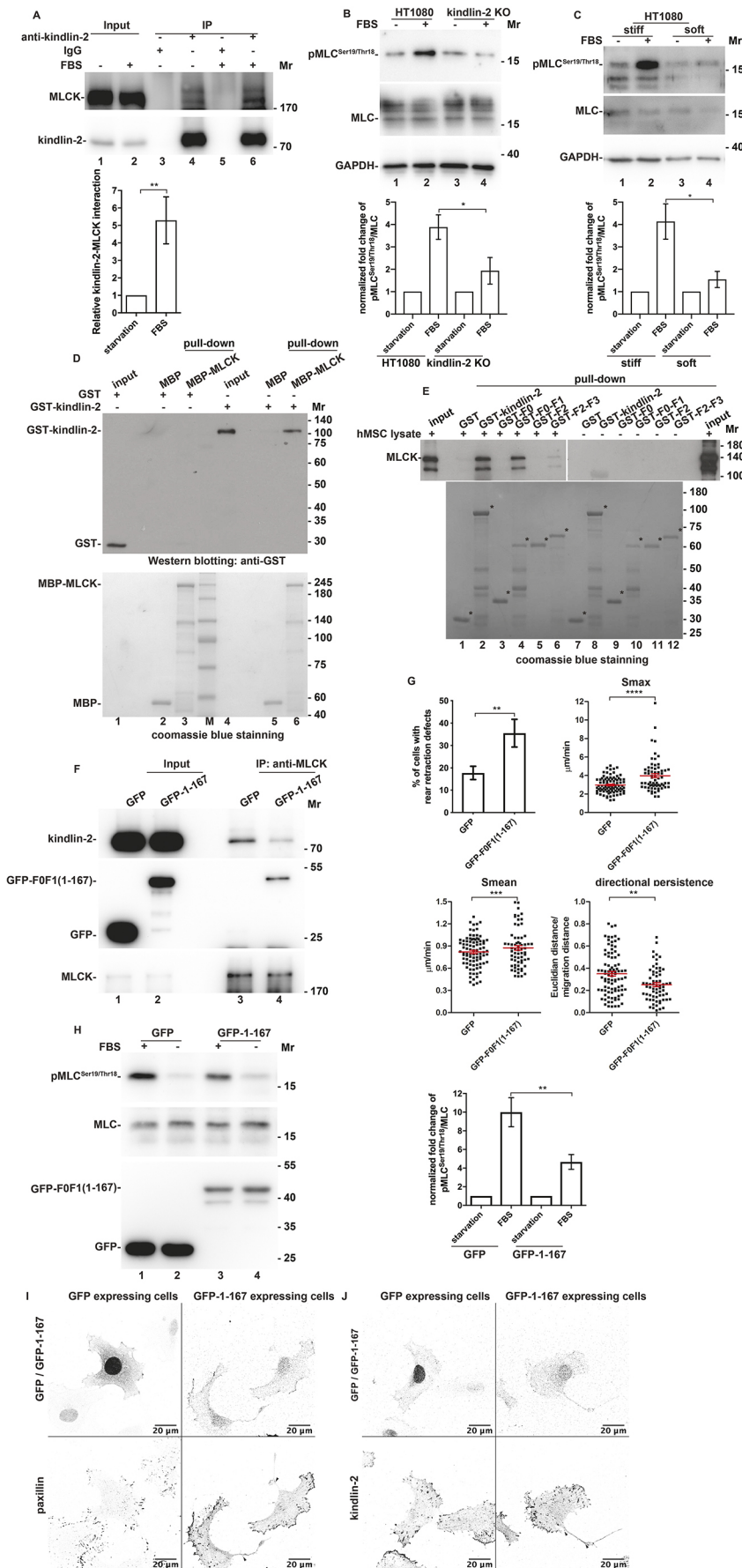
Fig. 7. Kindlin-2 interacts with MLCK directly and the interaction is enhanced upon serum-stimulation.
(A) HT1080 cells were either serum-starved (-) for 24 h or serum-starved for 24 h and then stimulated with FBS (+) for 5 min. Anti-kindlin-2 antibody was used to immunoprecipitate kindlin-2. Levels of MLCK co-immunoprecipitated with kindlin-2 were analyzed by western blotting and quantified ($n=4$, **$P<0.01$). The level of co-immunoprecipitated MLCK was increased upon serum stimulation. (B) Cells were prepared as described for A and analyzed by western blotting. Levels of pMLC[Ser19/Thr18] and the fold change of pMLC[Ser19/Thr18] levels in response to serum stimulation versus starvation were quantified for wild-type HT1080 and kindlin-2 KO cells, respectively ($n=4$, *$P<0.05$). The pMLC[Ser19/Thr18] level was increased in response to serum stimulation in HT1080 wild-type but not kindlin-2 KO cells. (C) HT1080 cells on soft and stiff matrices coated with collagen I were prepared and analyzed as in B ($n=3$, *$P<0.05$). The pMLC[Ser19/Thr18] level was increased in response to serum stimulation in HT1080 cells plated on stiff but not soft matrices. (D) Pulldown assays with MBP-MLCK pulling down GST-kindlin-2. The samples were analyzed by western blotting with anti-GST (top) or Coomassie Blue staining (bottom). (E) Pulldown assay of GST-kindlin-2 (full-length), GST-F0-F1, GST-F2 or GST-F2-F3 for MLCK from human mesenchymal stem cells. Samples were analyzed by western blotting using anti-MLCK antibody (top) or Coomassie Blue staining (bottom); positions of GST-fusion proteins are indicated by asterisks. GST-F0-F1, like GST-kindlin-2, could pull down MLCK. (F) HT1080 cells were transfected with GFP-F0F1 (aa 1–167) or GFP. Anti-MLCK antibody was used to immunoprecipitate MLCK. Kindlin-2 and GFP-F0F1 (aa 1–167) co-immunoprecipitated with MLCK were detected by anti-kindlin-2 and anti-GFP antibodies, respectively. (G) Cell migration analysis. Top left: percentage of cells showing rear retraction defects during migration (see Movie 14). Top right and all panels below: mean and maximum migration speed (Smean and Smax, respectively), and directional persistence of HT1080 cells overexpressing GFP-F0F1 (aa 1–167) or GFP only. Data are shown as mean±s.e.m. [GFP, $n=90$; GFP-F0F1 (aa 1–167), $n=66$]. Smax and Smean were increased while directional persistence was decreased in GFP-F0F1 (aa 1–167) expressing cells. **$P<0.005$, ***$P<0.0001$, ****$P<0.0001$. (H) HT1080 cells were transfected with GFP-F0F1 (aa 1–167) or GFP, and cells were serum-starved (-) or stimulated with FBS (+) as described in A, and analyzed by western blotting using antibodies as indicated (left panel). The fold change of pMLC[Ser19Thr18] in response to serum stimulation versus starvation was quantified (right panel, $n=3$, *$P<0.05$, **$P<0.005$). The fold change of pMLC[Ser19/Thr18] in response to serum stimulation was reduced in GFP-F0F1 (aa 1–167)-expressing cells. (I,J) HT1080 cells were transfected with GFP-F0F1 (aa 1–167) or GFP (upper panels). The cells were stained with anti-paxillin (I) or anti-kindlin-2 (J) antibodies (lower panels). Scale bars: 20 μm. Paxillin or kindlin-2 detected in the stretched retracting rear of GFP-F0F1 (aa 1–167)-expressing cells are indicated by arrowheads.
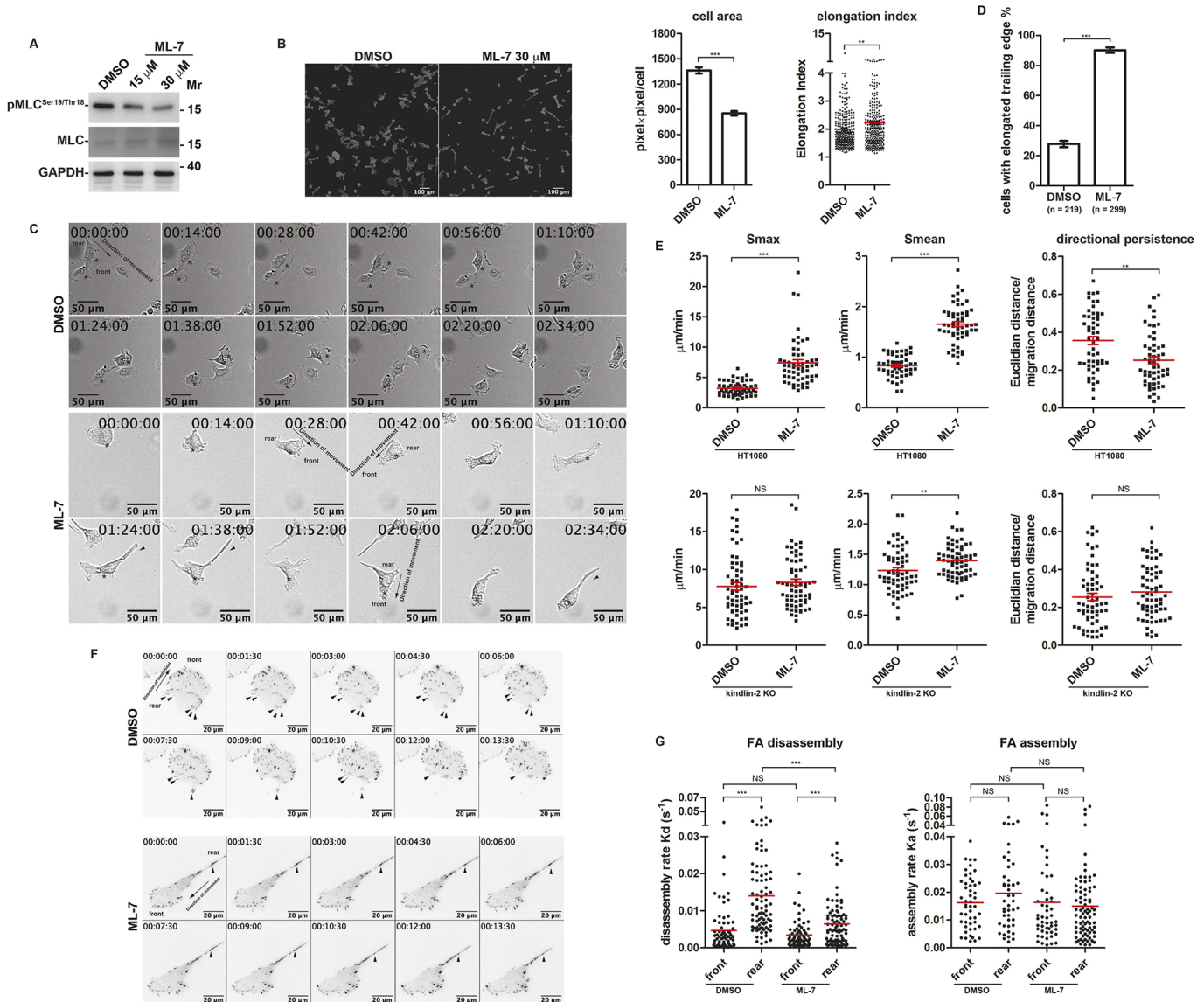
Fig. 8. Inhibition of MLCK causes defects on cell shape change, cell migration and rear FA disassembly, resembling those of kindlin-2-deficient cells.
(A) Western blotting of pMLC$^{Ser19/Thr18}$ in cells treated with DMSO or ML-7 (15 µM or 30 µM) for 2 h. The level of pMLC$^{Ser19/Thr18}$ was reduced in ML-7-treated cells. (B) HT1080 cells plated on fibronectin and treated with DMSO or ML-7 (30 µM) for 2 h were analysed for cell spreading and morphology. Cells were stained with Alexa647-conjugated phalloidin. Cell spreading area and elongation index were quantified (right). DMSO (n=292), ML-7 (n=285). Cell area was reduced and elongation index was increased in ML-7-treated cells. **P<0.005, ***P<0.0001. Scale bars: 100 µm. (C) Time-lapse live-cell images of migrating HT1080 cells treated with ML-7 or DMSO (see Movie 16). Scale bars: 50 µm. The cells tracked are marked by asterisk. Arrowheads indicate elongated trailing edge in ML-7-treated cells during migration. (D) Quantification of cells with elongated trailing edge (in %) (see Movies 15,16). Data are shown as mean±s.e.m. ***P<0.0001. (E) Quantification of migration Smax, Smean and directional persistence of DMSO- or ML-7-treated wild-type HT1080 and kindlin-2 KO cells, respectively (see Movies 15,16). Data are shown as mean±s.e.m. Smax was increased and directional persistence was decreased in ML-7-treated HT1080 wild-type but not kindlin-2 KO cells. **P<0.005, ***P<0.0001, NS: not significant. (F) Time-lapse TIRF images of paxillin-Ruby2 (arrowheads) in DMSO or ML-7 treated HT1080 cells (see Movie 17). Scale bars: 20 µm. (G) Quantification of FA disassembly (K_d) and assembly (K_a) rates in the front and rear region of migrating cells treated with DMSO or ML-7. The mean is plotted in red. DMSO-treated cells: at cell front K_d=0.0047±0.0007 s^{-1} (n=71) and K_a=0.015±0.001 s^{-1} (n=69), at cell rear K_d=0.014±0.001 s^{-1} (n=86) and K_a=0.020±0.002 s^{-1} (n=46). ML-7-treated cells: at cell front K_d=0.0035±0.0004 s^{-1} (n=74) and K_a=0.016±0.002 s^{-1} (n=51), at cell rear K_d=0.065±0.0007 s^{-1} (n=91) and K_a=0.015±0.0016 s^{-1} (n=83). K_d at the cell rear was reduced in ML-7-treated cells. ***P<0.0005, NS: not significant.

conserved component of FAs – is a key regulator of rear FA sliding and disassembly, and of rear retraction during cell migration.

By analyzing FA dynamics at the front and rear, we showed that FA disassembly is spatially polarized in migrating cells, i.e. at the rear, FAs exhibited adhesion sliding and a significantly higher disassembly rate as compared to those at the front, thereby facilitating effective trailing edge detachment and directional persistence (Fig. 5, Movie 9). Kindlin-2 deficiency impaired rear retraction (Movies 2–7), FA sliding and disassembly at the rear (Movie 9), resulting in loss of spatially polarized pattern of FA disassembly (Fig. 5). Kindlin-2-deficient cells exhibited a decrease in directional persistence, which depends on correct front-rear polarization (Fig. 4). These findings explain why the shape of kindlin-2-deficient cells is severely elongated (Fig. 2), and raise the interesting question as to how kindlin-2 exerts effects on front-rear polarization and directional persistence in migrating cells.

There is substantial evidence suggesting that actomyosin contractility plays crucial roles in establishing and maintaining front-rear polarity and rear retraction of the cell (Sanchez-Madrid and Serrador, 2009; Ladoux et al., 2016). We recently found that kindlin-2 associates with MLCK (Guo et al., 2018). In the current study, we have shown that kindlin-2 directly interacts with MLCK (Fig. 7C). Furthermore, we have assessed the role of kindlin-2 in regulation of localized tension at FAs. Serum is known to promote actomyosin-dependent forces (Burridge and Guilluy, 2016). Indeed, in response to serum stimulation, TLN HP35 in HT1080 cells demonstrated a significantly higher tension at FAs (Fig. 6B). This, however, was lost in kindlin-2-deficient cells (Fig. 6B), suggesting that kindin-2 is crucial for serum-induced actomyosin contractility at FAs. At the molecular level, serum stimulation promoted the interaction between kindlin-2 and MLCK, as well as the phosphorylation of MLC (Fig. 7A,B). In kindlin-2 KO cells, the phosphorylation of MLC in response to serum stimulation was impaired (Fig. 7B) – reminiscent of the reduced phosphorylation of MLC in wild-type cells grown on soft matrices (Fig. 7C), which are known to reduce actomyosin contractility (Mih et al., 2012). These data provide an explanation as to why kindlin-2-deficient cells failed to develop serum-induced actomyosin-dependent tension at FAs. Similar to myosin IIA-deficient fibroblasts (Vicente-Manzanares et al., 2007, 2008), kindlin-2-deficient cells showed defective rear retraction and impaired adhesion disassembly at the rear (Figs 4 and 5). Additionally, inhibition of MLCK in wild-type cells induced an elongated morphology with impaired rear-end detachment (Fig. 8). Furthermore, consistent with previous studies (Worthylake et al., 2001; Webb et al., 2002, 2004), inhibition of MLCK significantly reduced the rate of rear FA disassembly (Fig. 8). Of note, the effects chemical inhibition of MLCK has on cell migration largely depended on the presence of kindlin-2 (Fig. 8). Finally, similar to kindlin-2 deficiency, inhibition of the interaction between kindlin-2 and MLCK in response to GFP-F0F1 (aa 1–167) resulted in suppression of serum-induced myosin activation and cell migration defects (Fig. 7F–I). Collectively, these results suggest that kindlin-2 is crucial for the regulation of MLC phosphorylation and actomyosin contraction, rear retraction and directional persistence in cell migration. However, our preliminary experiments, using purified MLCK, failed to show a requirement of kindlin-2 in the biochemical activation of MLCK in vitro (Fig. S7). Furthermore, overexpression of constitutively active MLCK in kindlin-2 KO cells failed to reverse the migration defects induced by the loss of kindlin-2 (Fig. S8). Thus, the fact that loss of kindlin-2 impairs serum-induced MLCK-mediated MLC phosphorylation in cells probably reflects a function of kindlin-2 in facilitating MLCK-mediated MLC phosphorylation in cells – rather than a direct requirement of kindlin-2 in the biochemical activation of MLCK.

We found that, although loss of kindlin-2 did not significantly affect FA dynamics in the front, it markedly reduced FA sliding and disassembly at the rear of cells (Fig. 5B). How does kindlin-2 accomplish this spatially distinct regulation of FA disassembly during cell migration? One possibility is that kindlin-2 is only involved in regulating relatively fast FA disassembly – i.e. that at the cell rear – which is accompanied by fast forward sliding (Movie 10). Force-induced cell polarization mainly depends on FA sliding, which is linked to RhoA-driven actomyosin machinery (Goldyn et al., 2009). Kindlin-1 and -2, and the complex between ILK, PINCH and parvin are involved in the regulation of Rac and Rho activities (Has et al., 2009; Theodosiou et al., 2016; Bottcher et al., 2017; Sun et al., 2017; Yasuda-Yamahara et al., 2018; Chronopoulos et al., 2020; Kadry et al., 2018; Montanez et al., 2009). We recently found that RhoA

activity is crucial for the formation of the kindlin-2–MLCK complex (Guo et al., 2018). However, we did not observe any significant alterations of the steady-state levels of Rac1 and RhoA activation in kindlin-2 KO HT1080 cells compared to those in wild-type HT1080 cells (Fig. S8C). We also analyzed RhoA activation in migrating cells by using a FRET-based RhoA activity sensor and did not observe a significant reduction of RhoA activation in kindlin-2 KO HT1080 cells compared to that in wild-type HT1080 cells (Fig. S8D). Loss of kindlin-2 appeared to slightly reduce serum stimulation-induced RhoA activation, although this was not statistically significant (Fig. S8E). Although the role of kindlin-2 in local – i.e. cell rear – activation of Rac1 and RhoA remains to be determined in future studies, previous research has shown that actomyosin contraction is a dominant force driving cell rear retraction when large forces are required (Cramer, 2013). Actomyosin contraction is increased in response to microtubule-induced release of Rho GEFs, resulting in increased FA disassembly (Zenke et al., 2004; Kwan and Kirschner, 2005). Thus, actomyosin contractility may help break adhesive interactions during cell migration (Jay et al., 1995), and an increase in actomyosin contractility is likely to be needed for FA disassembly and rear detachment (Broussard et al., 2008). In this regard, it is worth noting that kindlin-2 is crucial for serum-stimulated actomyosin contraction at FAs (Fig. 6B), although it is dispensable for the basal tension (Fig. 6C) under resting conditions. These results suggest that a locally increased actomyosin contractile activity, coupled with rear-edge retraction, is likely to be required to rip off rear FAs from the substratum in order to promote efficient cell migration (Webb et al., 2004; Lauffenburger and Horwitz, 1996). Interestingly, similar to kindlin-2 deficiency (Fig. 5), serum deprivation also selectively impaired FA disassembly at the cell rear, which was released after serum stimulation (Fig. 6D,E). The serum deprivation-induced impairment of rear FA disassembly is consistent with the notion that actomyosin activity is crucial for adhesion release at the rear to ensure efficient cell migration (Ladoux et al., 2016). Because spatially distinct FA dynamics correlate to directional migration (Mohl et al., 2012), this kindlin-2-mediated regulation of polarized FA disassembly provides an explanation as to why kindlin-2 deficiency significantly reduced directional persistence during cell migration (Fig. 4).

Cell migration is a complex process that requires the coordinated regulation of multiple processes. Although our study provides strong evidence that kindlin-2 exerts functions in promoting rear FA disassembly and directional persistence through regulation of actomyosin contraction, our results also support that other processes in which kindlin-2 is involved, such as regulation of cell surface integrin levels and cell substratum traction forces, are pertinent to cell migration as well. For example, consistent with a role of kindlins in the regulation of cell-surface integrin levels (Harburger et al., 2009; Margadant et al., 2013, 2012; Kruger et al., 2008; Qu et al., 2011; Schmidt et al., 2011), we found that, in response to loss of kindlin-2, cell surface levels of αVβ3 integrin were reduced, whereas those of α2 and β1 integrins were modestly increased (Fig. S1). Furthermore, loss of kindlin-2 markedly reduced the number of FAs (Fig. 3B), which also influences substratum traction, force exerted on the cell. These changes might also contribute to the migration defects found in kindlin-2-deficient cells. Indeed, migration speed, an important parameter of migratory behavior, is determined by both cellular contractile forces and substratum traction forces exerted on cell–ECM adhesions (Lauffenburger and Horwitz, 1996). Theoretically, the ratio of contractile force to substratum traction force influences migration speed in a biphasic manner (Dimilla et al., 1991). Maximal

migration speed appears to correlate inversely with contractile force (Oliver et al., 1994). Kindlin-2 deficiency not only reduced directional persistence but also increased maximum migration speed (Fig. 4C, Fig. S1). Thus, the increased migration speed associated with kindlin-2-deficient cells might result not only from reduced contractile forces but also from altered cell surface integrin levels (Fig. S1) and weakened binding activity between integrin and ligand – as kindlin-2 is known to be crucial for integrin activation and cell-ECM adhesion (Shi et al., 2007; Larjava et al., 2008; Li et al., 2017; Ma et al., 2008).

Although they share considerable sequence similarity, kindlin-2 and -1 are encoded by different genes (Larjava et al., 2008). Furthermore, the tissue expression pattern and cellular functions of these two kindlins differ significantly (Rognoni et al., 2016; Plow et al., 2009; Bandyopadhyay et al., 2012). In this study, we also investigated the role of kindlin-1 in the regulation of cell migration. Unlike that of kindlin-2, depletion of kindlin-1 did not significantly affect cell shape and cell spreading in HT1080 cells (Fig. 1). This could be due to the difference in either functions or expression levels of these two kindlins. When GFP-tagged kindlin-1 was expressed in kindlin-2 KO cells at a level similar to GFP-kindlin-2, GFP-kindlin-1, like GFP-kindlin-2, could functionally rescue defects of kindlin-2 KO cells in cell spreading (Fig. 2), rear retraction (Movie 8) and rear FA disassembly (Fig. 5C, Movie 10). Moreover, MLCK can co-precipitate with either GFP-kindlin-1 or -2 (Fig. S6). Thus, the defects in cell spreading and migration caused by lack of kindlin-2 in HT1080 cells are probably due to the fact that kindlin-1 levels are insufficient to counteract this loss and to support these processes. Moreover, it appears that kindlin-1 and -2 share considerably functional redundancy in the regulation of these processes. Our findings, however, do not rule out that the functions of kindlin-1 or -2 may differ in regard to other processes. Thus, the vastly different consequences caused by genetic ablation of kindlin-1 or kindlin-2 are likely to reflect the differences regarding their function(s) in certain cellular processes but also their expression pattern in cells and tissues (Ussar et al., 2008; Postel et al., 2013; Huet-Calderwood et al., 2014; Lai-Cheong et al., 2008; Margadant et al., 2013; He et al., 2011; Harburger et al., 2009).

MATERIALS AND METHODS
DNA constructs
The CRISPR/Cas9 plasmid pSpCas9n (BB)-2A-GFP (PX461) was obtained from Addgene (#48140), deposited by Feng Zhang (Ran et al., 2013), to which the following oligonucleotides were annealed and ligated: kindlin-1 guide A1: 5′-caccgCTTCATTGGGGATGGTCAACG-3′; kindlin-1 guide A2: 5′-aaacCGTTGACCATCCCAATGAAGc-3′; kindlin-1 guide B1: 5′-caccg-ACGTCACACTGAGAGTATC-3′; kindlin-1 guide B2: 5′-aaacGATACTC-TCAGTGTGACGTc-3′; kindlin-2 guide A1: 5′-caccgCACCTCGCCGGT-CACTCTCA-3′; kindlin-2 guide A2: 5′-aaacTGAGAGTGACCGGCGAG-GTGc-3′; kindlin-2 guide B1: 5′-caccgTGGAGGCGTGATGCTTAAGCT-GG-3′; kindlin-2 guide B2: 5′-aaacCCAGCTTAAGCATCACGCCTc-3′. Lowercase letters indicate overhang sequences for ligation into *Bbs1*-processed vector; uppercase letters indicate target site sequence.

Primers used to determine the disruption of human *FERMT1* (kindlin-1) or *FERMT2* (kindlin-2) are as follows:

kindlin-1 KO fw: 5′-TGGTCTTGGAGAAGTGGGTG-3′; kindlin-1 KO re: 5′-CCAGCCATTAGTGGTGATGC-3′; kindlin-2 KO fw: 5′-GAGTG-ACGCTTACGAGAGCC-3′; kindlin-2 KO re: 5′-GCATTTGCGAGATG-CCAAGA-3′.

Constructs encoding respective GFP-tagged wild-type kindlin-2, W619Q mutant and LK(47)/AA kindlin-2 have previously been

described (Li et al., 2017; Guo et al., 2018). GFP-tagged kindlin-1 was subcloned into pEGFP-C. The FRET-based talin tension-sensor system (TLN CTL, TLN Y, and TLN HP35) used to measure tension generated by actomyosin contractility was a kind gift from Dr Carsten Grashoff (Institute of Molecular Cell Biology, Münster, Germany) (Austen et al., 2015). The FRET-based RhoA sensor Clover-RhoA-PKN-mRuby2 was modified from a kind gift from Dr Michiyuki Matsuda (Department of Pathology and Biology of Diseases, Kyoto University, Japan) (Aoki and Matsuda, 2009).

Generation of kindlin-1, kindlin-2 KO cells
The CRISPR/Cas9 system targeting *kindlin-1* or *kindlin-2* was transfected to human HT1080 fibroblasts using Lipofectamine 3000 transfection kit (Invitrogen) when the cell confluence had reached ∼80%. Twenty-four hours after transfection, single cells were sorted into 96-well plates according to expression of GFP. Single clones were isolated and examined to determine disruption of the targeted locus.

Cell culture
Wild-type, kindlin-2 KO or kindlin-1 KO HT1080 cells were cultured in minimum essential medium (MEM; CORNING) supplemented with 10% fetal bovine serum (FBS, PAN BIOTECH), 1× non-essential amino acid (NEAA) solution (Gibco), and penicillin-streptomycin (100 U/ml) solution (HyClone Laboratories). The cells were digested using 0.25% trypsin-EDTA (Gibco) and passaged at 1:8 and incubated at 37°C (5% CO_2) for 48 h. Human podocytes, mesenchymal stem cells and A549 lung adenocarcinoma cells were cultured as described previously (Guo et al., 2018, 2019; Sun et al., 2017). For serum stimulation assays, cells were cultured in serum-deprived medium for 24 h, and then were stimulated with 10% FBS for 5, 15, 30 or 60 min. For the ML-7 treatment, 15 or 30 μM ML-7 (Selleck, #S8388) was used to treat cultured cells for 2 h.

Western blotting
Western blotting was performed as previously described (Guo et al., 2018). In brief, whole-cell protein extracts were obtained using 1× SDS (50 mM Tris-HCl pH 6.8, 2% SDS, 10% glycerol). The concentration of total proteins was determined using BCA protein assay kit (Pierce). 20–30 μg protein was loaded per lane. Proteins were separated by SDS-PAGE and transferred to PVDF membrane (Millipore). The membranes were blocked with 5% BSA in Tris-buffered saline (50 mM Tris-HCl and 150 mM NaCl pH 7.4) containing 0.1% Tween 20 for 1 h at room temperature, followed by overnight incubation at 4°C with specific primary antibodies against kindlin-1 (1:1000; Cell Signaling Technology, #36734S), kindlin-2 (1:1000; proteintech, #11453-1-AP), MLC2 (1:1000 in 5% BSA; Cell Signaling Technology, #3672S), pMLC2[Ser19/Thr18] (1:1000 in 5% BSA; Cell Signaling Technology, #3674S), MLCK (1:10,000; Sigma, #M7905), and GAPDH (1:10,000; ZSGB-BIO, #TA-08). After washing and incubation with the appropriate horseradish peroxidase (HRP)-conjugated anti-mouse (1:10,000; #711-005-152) or anti-rabbit (1:10,000; #715-005-151) secondary antibody (both Jackson ImmunoResearch), blots were developed using an ECL kit (Bio-Rad) and then exposed to X-ray film (Super RX-N-C, Fuji Film). The images were scanned using an imaging scanning system (L365, EPSON Scan).

Co-immunoprecipitation assay
Cells were lysed with immunoprecipitation (IP) lysis buffer (Beyotime, #P0013) containing 1 mM PMSF. After incubation on ice for 30 min and centrifugation for 15 min at 4°C, the supernatants were collected. Total protein (0.5 mg) from each sample was used for co-immunoprecipitation assay. The cell lysates were pre-cleaned by incubation with 15 μl of Protein A/G plus beads (sc-2003, Santa Cruz) at 4°C for 30 min, followed by addition of 1 μl anti-kindlin-2 antibody (3A3.5) or 3 μl of unspecific mouse IgG (Santa Cruz, sc-2025) as a negative control and incubation at 4°C for 2 h. The samples were then mixed with Protein A/G PLUS-Agarose beads (15 μl/sample), incubated overnight, followed by washing (5×) with lysis buffer. The precipitates were eluted with 2× Laemmli loading buffer and subjected to western blotting with antibodies as specified.

GST-fusion and MBP-fusion protein binding assays

Direct association of kindlin-2 with MLCK was analyzed by using recombinant glutathione S-transferase (GST)-tagged to kindlin-2 and MBP-MLCK (also containing a His-tag) fusion proteins in pulldown assays as previously described (Guo et al., 2018). Briefly, 5 µg of purified MBP-MLCK fusion protein was incubated with 10 µg of GST-kindlin-2 [GST-F0 (aa 1–98), GST-F0-F1 (aa 1–280), GST-F2 (aa 281–565) and GST-F2-F3 (aa 281–680), respectively] or GST (as a negative control) bound to 20 µl of Glutathione Sepharose 4B (GE Healthcare) in the binding buffer (PBS supplemented with 1% TritonX-100; total mixture volume=1.5 ml). Reciprocally, 5 µg of purified GST-kindlin-2 fusion proteins were mixed with 6 µg of MBP-MLCK or MBP (as a negative control) bound to 20 µl of Amylose Resin (NEB) in the binding buffer (total mixture volume=1.5 ml). The respective mixtures were incubated at 4°C for 2 h, followed by washing once with binding buffer and twice with PBS. After the last wash, the beads were mixed with 25 µl of 2× sample buffer and boiled at 95°C for 5 min. MBP- (or GST-) tagged proteins bound to GST-kindlin-2 (or MBP-MLCK) were detected by western blotting with anti-His (or anti-GST) antibodies.

Live-cell imaging and cell migration analysis

Cells were seeded in Nunc Lab-Tek II chambered coverglasses (Merck, Nalge Nunc, 3000 cells/chamber) and placed in a heated and air humidified chamber built in a Nikon inverted microscope TE2000E. Phase-contrast time-lapse imaging was carried out at 1.5-min or 2-min intervals for 1–3 h for HT1080 cells and at 4-min intervals for 1–3 h for human podocytes and A549 cells. Images were captured on the microscope with a 10× Ph1 objective (0.65 µm/pixel), perfect focus system (PFS), and Hamamatsu C-11440-22cU camera controlled by NIS-elements software (Nikon). Image stacks were processed and migrating cells were manually tracked using ImageJ software (NIH). The mean and maximum migration speed (Smean and Smax, respectively) as well as directional persistence were analyzed using the Chemotaxis and Migration Tool from ibidi.

Immunofluorescence staining

Cells seeded on coverslips coated with 5 µg/ml fibronectin or 5 µg/ml collagen were fixed with 4% PFA+0.25% Triton-X 100 and washed 3× with PBS. 50 mM NH₄Cl was used to decrease the background fluorescence. After washing 3× with PBS and blocking with the blocking buffer (5% BSA with 0.1% Triton-X 100 in PBS), the cells were incubated with antibodies against paxillin (1:300; Cell Signaling Technology, #2542S) or kindlin-2 (1:500; clone 3A3.5), or Alexa Fluor 488-, 555- or 647-conjugated phalloidin for 1 h at room temperature. The cells stained with primary antibodies were then washed 3× with the blocking buffer and incubated with Alexa Fluor 488- or 647-conjugated goat anti-rabbit or mouse IgG (H+L) (Life Technologies) secondary antibodies. After washing 3× with blocking buffer and PBS, coverslips were mounted with Prolong Gold antifade reagent (Invitrogen, P36934). Images were acquired using a Nikon A1R confocal fluorescence microscope with a 20× dry objective, 100× oil objective, or a Nikon total internal reflection fluorescence (TIRF) microscope with a 60× or 100× oil objective.

Measurement of cell elongation index

Ferret's diameter along the long (length) and short (width) dimension of cells stained with Alexa Fluor 488- or 555-conjugated phalloidin (actin) was measured using image analysis software Image-Pro-Plus (Median Cybemetics). The elongation index was defined as the length-to-width ratio.

TIRF imaging and analysis of cell-ECM adhesion dynamics

HT1080 wild-type or kindlin-2 KO cells stably expressing paxillin-mRuby2 were seeded into 8-well Nunc™ Lab-Tek™ II Chambered Coverglass (Thermofisher Scientific, Waltham, MA). Time-lapse TIRF imaging of FAs was performed as described (Stehbens and Wittmann, 2014). In brief, cells were imaged by using a Nikon TiE microscope equipped with a TIRF system using a CFI SR Apo TIRF 60xH (NA=1.49) oil immersion objective and an Andor iXon DU-897 EMCCD (Andor) under control of NIS-elements software (Nikon). Time-lapse fluorescence images of paxillin-mRuby2 excited by a 561 nm laser (or GFP-kindlin excited by a 488 nm laser) were collected every 45 s, and fluorescence intensity of mRuby2-paxillin or GFP-kindlin-2 at each FA was tracked using NIS-elements software (Nikon). Fluorescence intensity as a function of time was fitted with a sigmoidal and mono-exponential decay function during respective assembly and disassembly phase using SigmaPlot 12 (Systat Software Inc., San Jose, CA) and GraphPad Prism 6.0 (GraphPad Software, San Diego, CA) (Waters and Wittmann, 2014).

FRET-based talin tension sensor

TLN HP35, the FRET-based talin tension sensor, has been described previously (Austen et al., 2015). In brief, the TLN HP35 probe contains the 35 aa-long villin headpiece peptide (HP35), an ultrafast-folding peptide that responds to mechanical forces, inserted into the unstructured linker region between the head and rod domains of mouse talin-1. A YPet/mCherry pair of fluorophores flanking the HP35 sequence allows FRET measurements, which indicate mechanical tension that talin bears. The fluorescence lifetime (τ) of YPet was measured to calculate the FRET efficiency at given conditions. For comparison, τ of two controls, i.e. the talin wild-type control TLN Y in which only YPet is C-terminally tagged to talin-1, and the zero-force control TLN CTL in which HP35 and the YPet/mCherry pair are tagged to the C-terminus of talin-1, were measured in parallel. Because forces are not exerted on HP35 tagged to the C-terminus of talin-1, the YPet/mCherry pair in TLN CTL exhibits FRET.

Time-correlated single-photon fluorescence lifetime microscopy (TCSPC-FLIM)

TCSPC-FLIM experiments were performed as described previously (Austen et al., 2015). In brief, HT1080 wild-type or kindlin-2 KO cells were transiently transfected with TLN CTL, TLN Y or TLN HP35, and incubated in MEM in the absence of FBS for 24 h. Cells were then activated with MEM supplemented with 10% FBS for the different time durations, i.e. 5 min, 15 min and 30 min. Cells were fixed with 4% PFA and fluorescence images were recorded using a Nikon A1R confocal microscope equipped with a 485 nm pulsed diode laser (PDL 800-D, PicoQuant), a photodetector (PMA Hybrid 40, PicoQuant), and a 100× oil objective. Detection was carried out over a time window of 44 ns after the excitation pulse with the TCSPC resolution of 25.0 ps.

For each group of cells, 7–16 cells were analyzed per experiment. Data analysis was performed using the SymPhoTime 64 software (PicoQuant). In brief, 'n-Exponential Tailfit' was selected as the fitting model, signals on FAs were selected as ROIs, and 'calculated IRF' was selected as initial fit to get the lifetime value (τ_{amp}). FRET efficiency was calculated as FRET efficiency=$1-\tau_{DA}/\tau_D$, where τ_D is the fluorescence lifetime of TLN Y and τ_{DA} is the fluorescence lifetime of TLN HP35 or TLN CTL.

Preparation of polyacrylamide hydrogels with different stiffness

Polyacrylamide hydrogels of different stiffness coated with collagen I (3 µg/ml) were prepared as published previously (Guo et al., 2018). Hydrogels containing 0.3% and 0.03% bis-acrylamide were regarded as stiff and soft matrices, respectively.

Flow cytometry

Cell surface expression levels of α2(CD49b), αVβ3(CD51/CD61) and β1(CD29) integrins in wild-type and kindlin-2 KO HT1080 cells were detected by using a BD FACS cytometer and analysed with FlowJo software as described previously (Theodosiou et al., 2016). Briefly, cells were plated on a fibronectin-coated (5 µg/ml) Petri dish overnight, trypsinized and washed with cold FACS buffer (30 mM Tris pH 7.4, 3% BSA, 180 mM NaCl, 1 mM MgCl₂, 1 mM CaCl₂, 3.5 mM KCl). 5×10⁵ cells were incubated with 3 µl fluorochrome-conjugated primary antibody (FITC anti-human CD49b, 1:33; FITC anti-human CD51/CD61, 1:33; or FITC Control IgG from eBioscience; Alexa Fluor 488 anti-human CD29, 1:33; and Alexa Fluor 488 control IgG from Biolegend) diluted in 100 µl of cold FACS buffer on ice for 1 h, and washed twice with FACS buffer before analysis.

Rac and RhoA activation assay

Rac1 and RhoA G-LISA activation assays were performed following the manufacturer's protocols (Cell Signaling). Additionally, the FRET sensor of

RhoA activation (Raichu-RhoA-CR) from Michiyuki Matsuda was modified using Clover-RhoA-PKN-mRuby2, and was then utilized to assess RhoA activation in live cells as previously described (Guo et al., 2018).

In vitro MLCK kinase assay

In vitro MLCK kinase activity was assessed using recombinant MBP-MLCK and His-MLC2 (human RLC, NP291024.1) fusion proteins as previously described (Baumann et al., 2017). Briefly, 10 nM purified MBP-MLCK and 10 μM His-MLC2 were incubated with 500 μM ATP (Sigma, #A2382) in 20 mM HEPES pH 7.5, 50 mM NaCl, 10 mM $MgCl_2$, 1 mM DTT, with or without 40 nM calmodulin (CaM, Sigma)/1 mM $CaCl_2$ in the presence of 40 nM GST-tagged kindlin-2 or GST as control at 37°C for 5, 20 or 60 min. Reactions were quenched by addition of SDS sample buffer. Levels of phosphorylated and total MLC2 were analyzed by western blotting using antibodies against pMLC2 Ser19 (Cell Signaling Technology #3671) and His-tag (Transgen #AB102-02).

In vitro CaM-MLCK binding assay

The effect of kindlin-2 on the interaction between MLCK and CaM was analyzed using MBP-MLCK pulldown assay following a previously described protocol (Guo et al., 2018). Briefly, 50 nM MBP-MLCK or MBP bound to amylose-resin was incubated with 400 nM GST-kindlin-2 or GST as control at 4°C for 60 min, followed by incubation with100 nM CaM (Sigma #C4874) and 10 mM $CaCl_2$ at 4°C for 30 min. Levels of CaM bound to MBP-MLCK in the presence or absence of GST-kindlin-2 were detected by western blotting with anti-CaM antibodies (Cell Signaling Technology, #35944).

Statistical analysis

Statistical data analysis for statistical significance was done using one- or two-tailed paired *t*-tests (GraphPad Prism version 5.00 for Windows, GraphPad Software, La Jolla, CA).

References
Adelstein, R. S. (1982). Calmodulin and the regulation of the actin-myosin interaction in smooth muscle and nonmuscle cells. *Cell* 30, 349-350. doi:10.1016/0092-8674(82)90232-x

Aoki, K. and Matsuda, M. (2009). Visualization of small GTPase activity with fluorescence resonance energy transfer-based biosensors. *Nat. Protoc.* 4, 1623-1631. doi:10.1038/nprot.2009.175

Austen, K., Ringer, P., Mehlich, A., Chrostek-Grashoff, A., Kluger, C., Klingner, C., Sabass, B., Zent, R., Rief, M. and Grashoff, C. (2015). Extracellular rigidity sensing by talin isoform-specific mechanical linkages. *Nat. Cell Biol.* 17, 1597-1606. doi:10.1038/ncb3268

Avraamides, C. J., Garmy-Susini, B. and Varner, J. A. (2008). Integrins in angiogenesis and lymphangiogenesis. *Nat. Rev. Cancer* 8, 604-617. doi:10.1038/nrc2353

Bandyopadhyay, A., Rothschild, G., Kim, S., Calderwood, D. A. and Raghavan, S. (2012). Functional differences between kindlin-1 and kindlin-2 in keratinocytes. *J. Cell Sci.* 125, 2172-2184. doi:10.1242/jcs.096214

Baumann, F., Bauer, M. S., Rees, M., Alexandrovich, A., Gautel, M., Pippig, D. A. and Gaub, H. E. (2017). Increasing evidence of mechanical force as a functional regulator in smooth muscle myosin light chain kinase. *Elife* 6, e26473. doi:10.7554/eLife.26473.032

Bledzka, K., Bialkowska, K., Sossey-Alaoui, K., Vaynberg, J., Pluskota, E., Qin, J. and Plow, E. F. (2016). Kindlin-2 directly binds actin and regulates integrin outside-in signaling. *J. Cell Biol.* 213, 97-108. doi:10.1083/jcb.201501006

Bottcher, R. T., Veelders, M., Rombaut, P., Faix, J., Theodosiou, M., Stradal, T. E., Rottner, K., Zent, R., Herzog, F. and Fassler, R. (2017). Kindlin-2 recruits paxillin and Arp2/3 to promote membrane protrusions during initial cell spreading. *J. Cell Biol.* 216, 3785-3798. doi:10.1083/jcb.201701176

Bretscher, M. S. (2008). On the shape of migrating cells–a 'front-to-back' model. *J. Cell Sci.* 121, 2625-2628. doi:10.1242/jcs.031120

Broussard, J. A., Webb, D. J. and Kaverina, I. (2008). Asymmetric focal adhesion disassembly in motile cells. *Curr. Opin. Cell Biol.* 20, 85-90. doi:10.1016/j.ceb.2007.10.009

Burridge, K. and Guilluy, C. (2016). Focal adhesions, stress fibers and mechanical tension. *Exp. Cell Res.* 343, 14-20. doi:10.1016/j.yexcr.2015.10.029

Chi, Q., Yin, T., Gregersen, H., Deng, X., Fan, Y., Zhao, J., Liao, D. and Wang, G. (2014). Rear actomyosin contractility-driven directional cell migration in three-dimensional matrices: a mechano-chemical coupling mechanism. *J. R Soc. Interface* 11, 20131072. doi:10.1098/rsif.2013.1072

Chronopoulos, A., Thorpe, S. D., Cortes, E., Lachowski, D., Rice, A. J., Mykuliak, V. V., Rog, T., Lee, D. A., Hytonen, V. P. and Del Rio Hernandez, A. E. (2020). Syndecan-4 tunes cell mechanics by activating the kindlin-integrin-RhoA pathway. *Nat. Mater.* 19, 669-678. doi:10.1038/s41563-019-0567-1

Cramer, L. P. (2013). Mechanism of cell rear retraction in migrating cells. *Curr. Opin. Cell Biol.* 25, 591-599. doi:10.1016/j.ceb.2013.05.001

Dimilla, P. A., Barbee, K. and Lauffenburger, D. A. (1991). Mathematical-model for the effects of adhesion and mechanics on cell-migration speed. *Biophys. J.* 60, 15-37. doi:10.1016/S0006-3495(91)82027-6

Dubash, A. D., Menold, M. M., Samson, T., Boulter, E., Garcia-Mata, R., Doughman, R. and Burridge, K. (2009). Chapter 1. Focal adhesions: new angles on an old structure. *Int. Rev. Cell Mol. Biol.* 277, 1-65. doi:10.1016/S1937-6448(09)77001-7

Etienne-Manneville, S. (2008). Polarity proteins in migration and invasion. *Oncogene* 27, 6970-6980. doi:10.1038/onc.2008.347

Gallant, N. D., Michael, K. E. and Garcia, A. J. (2005). Cell adhesion strengthening: contributions of adhesive area, integrin binding, and focal adhesion assembly. *Mol. Biol. Cell* 16, 4329-4340. doi:10.1091/mbc.e05-02-0170

Goldyn, A. M., Rioja, B. A., Spatz, J. P., Ballestrem, C. and Kemkemer, R. (2009). Force-induced cell polarisation is linked to RhoA-driven microtubule-independent focal-adhesion sliding. *J. Cell Sci.* 122, 3644-3651. doi:10.1242/jcs.054866

Grenz, H., Carbonetto, S. and Goodman, S. L. (1993). Alpha 3 beta 1 integrin is moved into focal contacts in kidney mesangial cells. *J. Cell Sci.* 105, 739-751.

Guo, L., Cai, T., Chen, K., Wang, R., Wang, J., Cui, C., Yuan, J., Zhang, K., Liu, Z., Deng, Y. et al. (2018). Kindlin-2 regulates mesenchymal stem cell differentiation through control of YAP1/TAZ. *J. Cell Biol.* 217, 1431-1451. doi:10.1083/jcb.201612177

Guo, L., Cui, C. H., Zhang, K., Wang, J. X., Wang, Y. L., Lu, Y. X., Chen, K., Yuan, J. F., Xiao, G. Z., Tang, B. et al. (2019). Kindlin-2 links mechano-environment to proline synthesis and tumor growth. *Nat. Commun.* 10, 845. doi:10.1038/s41467-019-08772-3

Gupton, S. L. and Waterman-Storer, C. M. (2006). Spatiotemporal feedback between actomyosin and focal-adhesion systems optimizes rapid cell migration. *Cell* 125, 1361-1374. doi:10.1016/j.cell.2006.05.029

Harburger, D. S., Bouaouina, M. and Calderwood, D. A. (2009). Kindlin-1 and -2 directly bind the C-terminal region of beta integrin cytoplasmic tails and exert integrin-specific activation effects. *J. Biol. Chem.* 284, 11485-11497. doi:10.1074/jbc.M809233200

Has, C., Herz, C., Zimina, E., Qu, H. Y., He, Y. H., Zhang, Z. G., Wen, T. T., Gache, Y., Aumailley, M. and Bruckner-Tuderman, L. (2009). Kindlin-1 is required for RhoGTPase-mediated lamellipodia formation in keratinocytes. *Am. J. Pathol.* 175, 1442-1452. doi:10.2353/ajpath.2009.090203

He, Y., Esser, P., Heinemann, A., Bruckner-Tuderman, L. and Has, C. (2011). Kindlin-1 and –2 have overlapping functions in epithelial cells implications for phenotype modification. *Am. J. Pathol.* 178, 975-982. doi:10.1016/j.ajpath.2010.11.053

Horton, E. R., Byron, A., Askari, J. A., Ng, D. H. J., Millon-Fremillon, A., Robertson, J., Koper, E. J., Paul, N. R., Warwood, S., Knight, D. et al. (2015).

Definition of a consensus integrin adhesome and its dynamics during adhesion complex assembly and disassembly. *Nat. Cell Biol.* **17**, 1577-1587. doi:10.1038/ncb3257

Horwitz, A. R. and Parsons, J. T. (1999). Cell migration–movin' on. *Science* **286**, 1102-1103. doi:10.1126/science.286.5442.1102

Horwitz, R. and Webb, D. (2003). Cell migration. *Curr. Biol.* **13**, R756-R759. doi:10.1016/j.cub.2003.09.014

Huet-Calderwood, C., Brahme, N. N., Kumar, N., Stiegler, A. L., Raghavan, S., Boggon, T. J. and Calderwood, D. A. (2014). Differences in binding to the ILK complex determines kindlin isoform adhesion localization and integrin activation. *J. Cell Sci.* **127**, 4308-4321. doi:10.1242/jcs.155879

Huttenlocher, A. and Horwitz, A. R. (2011). Integrins in cell migration. *Cold Spring Harb. Perspect Biol.* **3**, a005074. doi:10.1101/cshperspect.a005074

Hynes, R. O. (2002). Integrins: bidirectional, allosteric signaling machines. *Cell* **110**, 673-687. doi:10.1016/S0092-8674(02)00971-6

Insall, R. H. and Machesky, L. M. (2009). Actin dynamics at the leading edge: from simple machinery to complex networks. *Dev. Cell* **17**, 310-322. doi:10.1016/j.devcel.2009.08.012

Itoh, K., Hara, T., and Shibata, H. (1992). Diphosphorylation of platelet myosin by myosin light chain kinase. *Biochim. Biophys. Acta* **1133**, 286-292. doi:10.1016/0167-4889(92)90049-h

Jay, P. Y., Pham, P. A., Wong, S. A. and Elson, E. L. (1995). A mechanical function of Myosin-Ii in cell motility. *J. Cell Sci.* **108**, 387-393.

Kadry, Y. A., Huet-Calderwood, C., Simon, B. and Calderwood, D. A. (2018). Kindlin-2 interacts with a highly conserved surface of ILK to regulate focal adhesion localization and cell spreading. *J. Cell Sci.* **131**, jcs221184. doi:10.1242/jcs.221184

Kanchanawong, P., Shtengel, G., Pasapera, A. M., Ramko, E. B., Davidson, M. W., Hess, H. F. and Waterman, C. M. (2010). Nanoscale architecture of integrin-based cell adhesions. *Nature* **468**, 580-584. doi:10.1038/nature09621

Kirfel, G., Rigort, A., Borm, B. and Herzog, V. (2004). Cell migration: mechanisms of rear detachment and the formation of migration tracks. *Eur. J. Cell Biol.* **83**, 717-724. doi:10.1078/0171-9335-00421

Kruger, M., Moser, M., Ussar, S., Thievessen, I., Luber, C. A., Forner, F., Schmidt, S., Zanivan, S., Fassler, R. and Mann, M. (2008). SILAC mouse for quantitative proteomics uncovers kindlin-3 as an essential factor for red blood cell function. *Cell* **134**, 353-364. doi:10.1016/j.cell.2008.05.033

Kwan, K. M. and Kirschner, M. W. (2005). A microtubule-binding Rho-GEF controls cell morphology during convergent extension of Xenopus laevis. *Development* **132**, 4599-4610. doi:10.1242/dev.02041

Ladoux, B., Mege, R. M. and Trepat, X. (2016). Front-rear polarization by mechanical cues: from single cells to tissues. *Trends Cell Biol.* **26**, 420-433. doi:10.1016/j.tcb.2016.02.002

Lai-Cheong, J. E., Ussar, S., Arita, K., Hart, I. R. and Mcgrath, J. A. (2008). Colocalization of kindlin-1, kindlin-2, and migfilin at keratinocyte focal adhesion and relevance to the pathophysiology of Kindler syndrome. *J. Invest. Dermatol.* **128**, 2156-2165. doi:10.1038/jid.2008.58

Larjava, H., Plow, E. F. and Wu, C. (2008). Kindlins: essential regulators of integrin signalling and cell-matrix adhesion. *EMBO Rep.* **9**, 1203-1208. doi:10.1038/embor.2008.202

Lauffenburger, D. A. and Horwitz, A. F. (1996). Cell migration: a physically integrated molecular process. *Cell* **84**, 359-369. doi:10.1016/S0092-8674(00)81280-5

Li, H. D., Deng, Y., Sun, K., Yang, H. B., Liu, J., Wang, M. L., Zhang, Z., Lin, J. R., Wu, C. Y., Wei, Z. Y. et al. (2017). Structural basis of kindlin-mediated integrin recognition and activation. *Proc. Natl. Acad. Sci. USA* **114**, 9349-9354. doi:10.1073/pnas.1703064114

Lou, S. S., Diz-Munoz, A., Weiner, O. D., Fletcher, D. A. and Theriot, J. A. (2015). Myosin light chain kinase regulates cell polarization independently of membrane tension or Rho kinase. *J. Cell Biol.* **209**, 275-288. doi:10.1083/jcb.201409001

Ma, Y. Q., Qin, J., Wu, C. and Plow, E. F. (2008). Kindlin-2 (Mig-2): a co-activator of beta3 integrins. *J. Cell Biol.* **181**, 439-446. doi:10.1083/jcb.200710196

Margadant, C., Kreft, M., De Groot, D. J., Norman, J. C. and Sonnenberg, A. (2012). Distinct roles of talin and kindlin in regulating integrin alpha5beta1 function and trafficking. *Curr. Biol.* **22**, 1554-1563. doi:10.1016/j.cub.2012.06.060

Margadant, C., Kreft, M., Zambruno, G. and Sonnenberg, A. (2013). Kindlin-1 regulates integrin dynamics and adhesion turnover. *PLoS ONE* **8**, e65341. doi:10.1371/journal.pone.0065341

Mierke, C. T., Rosel, D., Fabry, B. and Brabek, J. (2008). Contractile forces in tumor cell migration. *Eur. J. Cell Biol.* **87**, 669-676. doi:10.1016/j.ejcb.2008.01.002

Mih, J. D., Marinkovic, A., Liu, F., Sharif, A. S. and Tschumperlin, D. J. (2012). Matrix stiffness reverses the effect of actomyosin tension on cell proliferation. *J. Cell Sci.* **125**, 5974-5983. doi:10.1242/jcs.108886

Mohl, C., Kirchgessner, N., Schafer, C., Hoffmann, B. and Merkel, R. (2012). Quantitative mapping of averaged focal adhesion dynamics in migrating cells by shape normalization. *J. Cell Sci.* **125**, 155-165. doi:10.1242/jcs.090746

Montanez, E., Ussar, S., Schifferer, M., Bosl, M., Zent, R., Moser, M. and Fassler, R. (2008). Kindlin-2 controls bidirectional signaling of integrins. *Genes Dev.* **22**, 1325-1330. doi:10.1101/gad.469408

Montanez, E., Wickstrom, S. A., Altstatter, J., Chu, H. and Fassler, R. (2009). Alpha-parvin controls vascular mural cell recruitment to vessel wall by regulating RhoA/ROCK signalling. *EMBO J.* **28**, 3132-3144. doi:10.1038/emboj.2009.295

Northey, J. J., Przybyla, L. and Weaver, V. M. (2017). Tissue force programs cell fate and tumor aggression. *Cancer Discov.* **7**, 1224-1237. doi:10.1158/2159-8290.CD-16-0733

Oakes, P. W. and Gardel, M. L. (2014). Stressing the limits of focal adhesion mechanosensitivity. *Curr. Opin. Cell Biol.* **30**, 68-73. doi:10.1016/j.ceb.2014.06.003

Oliver, T., Lee, J. and Jacobson, K. (1994). Forces exerted by locomoting cells. *Semin. Cell Biol.* **5**, 139-147. doi:10.1006/scel.1994.1018

Parsons, J. T., Horwitz, A. R. and Schwartz, M. A. (2010). Cell adhesion: integrating cytoskeletal dynamics and cellular tension. *Nat. Rev. Mol. Cell Biol.* **11**, 633-643. doi:10.1038/nrm2957

Petrie, R. J., Doyle, A. D. and Yamada, K. M. (2009). Random versus directionally persistent cell migration. *Nat. Rev. Mol. Cell Biol.* **10**, 538-549. doi:10.1038/nrm2729

Plow, E. F., Qin, J. and Byzova, T. (2009). Kindling the flame of integrin activation and function with kindlins. *Curr. Opin Hematol.* **16**, 323-328. doi:10.1097/MOH.0b013e32832ea389

Pluskota, E., Dowling, J. J., Gordon, N., Golden, J. A., Szpak, D., West, X. Z., Nestor, C., Ma, Y. Q., Bialkowska, K., Byzova, T. and et al. (2011). The integrin coactivator kindlin-2 plays a critical role in angiogenesis in mice and zebrafish. *Blood* **117**, 4978-4987. doi:10.1182/blood-2010-11-321182

Postel, R., Margadant, C., Fischer, B., Kreft, M., Janssen, H., Secades, P., Zambruno, G. and Sonnenberg, A. (2013). Kindlin-1 mutant Zebrafish as an in vivo model system to study adhesion mechanisms in the epidermis. *J. Investig. Dermatol.* **133**, 2180-2190. doi:10.1038/jid.2013.154

Qu, H., Tu, Y., Shi, X., Larjava, H., Saleem, M. A., Shattil, S. J., Fukuda, K., Qin, J., Kretzler, M. and Wu, C. (2011). Kindlin-2 regulates podocyte adhesion and fibronectin matrix deposition through interactions with phosphoinositides and integrins. *J. Cell Sci.* **124**, 879-891. doi:10.1242/jcs.076976

Ran, F. A., Hsu, P. D., Wright, J., Agarwala, V., Scott, D. A. and Zhang, F. (2013). Genome engineering using the CRISPR-Cas9 system. *Nat. Protoc.* **8**, 2281-2308. doi:10.1038/nprot.2013.143

Rid, R., Schiefermeier, N., Grigoriev, I., Small, J. V. and Kaverina, I. (2005). The last but not the least: the origin and significance of trailing adhesions in fibroblastic cells. *Cell Motil. Cytoskeleton* **61**, 161-171. doi:10.1002/cm.20076

Ridley, A. J., Schwartz, M. A., Burridge, K., Firtel, R. A., Ginsberg, M. H., Borisy, G., Parsons, J. T. and Horwitz, A. R. (2003). Cell migration: integrating signals from front to back. *Science* **302**, 1704-1709. doi:10.1126/science.1092053

Rognoni, E., Ruppert, R. and Fassler, R. (2016). The kindlin family: functions, signaling properties and implications for human disease. *J. Cell Sci.* **129**, 17-27. doi:10.1242/jcs.161190

Sanchez-Madrid, F. and Serrador, J. M. (2009). Bringing up the rear: defining the roles of the uropod. *Nat. Rev. Mol. Cell Biol.* **10**, 353-359. doi:10.1038/nrm2680

Schmidt, S., Nakchbandi, I., Ruppert, R., Kawelke, N., Hess, M. W., Pfaller, K., Jurdic, P., Fassler, R. and Moser, M. (2011). Kindlin-3-mediated signaling from multiple integrin classes is required for osteoclast-mediated bone resorption. *J. Cell Biol.* **192**, 883-897. doi:10.1083/jcb.201007141

Shi, X., Ma, Y. Q., Tu, Y., Chen, K., Wu, S., Fukuda, K., Qin, J., Plow, E. F. and Wu, C. (2007). The MIG-2/integrin interaction strengthens cell-matrix adhesion and modulates cell motility. *J. Biol. Chem.* **282**, 20455-20466. doi:10.1074/jbc.M611680200

Stehbens, S. J. and Wittmann, T. (2014). Analysis of focal adhesion turnover: a quantitative live-cell imaging example. *Methods Cell Biol.* **123**, 335-346. doi:10.1016/B978-0-12-420138-5.00018-5

Sun, Y., Guo, C., Ma, P., Lai, Y., Yang, F., Cai, J., Cheng, Z., Zhang, K., Liu, Z., Tian, Y. et al. (2017). Kindlin-2 association with Rho GDP-dissociation inhibitor alpha suppresses rac1 activation and podocyte injury. *J. Am. Soc. Nephrol.* **28**, 3545-3562. doi:10.1681/ASN.2016091021

Sun, Z., Costell, M. and Fassler, R. (2019). Integrin activation by talin, kindlin and mechanical forces. *Nat. Cell Biol.* **21**, 25-31. doi:10.1038/s41556-018-0234-9

Swaminathan, V. and Waterman, C. M. (2016). The molecular clutch model for mechanotransduction evolves. *Nat. Cell Biol.* **18**, 459-461. doi:10.1038/ncb3350

Theodosiou, M., Widmaier, M., Bottcher, R. T., Rognoni, E., Veelders, M., Bharadwaj, M., Lambacher, A., Austen, K., Muller, D. J., Zent, R. et al. (2016). Kindlin-2 cooperates with talin to activate integrins and induces cell spreading by directly binding paxillin. *Elife* **5**, e10130. doi:10.7554/eLife.10130

Tu, Y., Wu, S., Shi, X., Chen, K. and Wu, C. (2003). Migfilin and Mig-2 link focal adhesions to filamin and the actin cytoskeleton and function in cell shape modulation. *Cell* **113**, 37-47. doi:10.1016/S0092-8674(03)00163-6

Ussar, S., Moser, M., Widmaier, M., Rognoni, E., Harrer, C., Genzel-Boroviczeny, O. and Fassler, R. (2008). Loss of Kindlin-1 causes skin atrophy and lethal neonatal intestinal epithelial dysfunction. *PLoS Genet.* **4**, e1000289. doi:10.1371/journal.pgen.1000289

Vicente-Manzanares, M., Zareno, J., Whitmore, L., Choi, C. K. and Horwitz, A. F. (2007). Regulation of protrusion, adhesion dynamics, and polarity by myosins IIA and IIB in migrating cells. *J. Cell Biol.* **176**, 573-580. doi:10.1083/jcb.200612043

Vicente-Manzanares, M., Koach, M. A., Whitmore, L., Lamers, M. L. and Horwitz, A. F. (2008). Segregation and activation of myosin IIB creates a rear in migrating cells. *J. Cell Biol.* **183**, 543-554. doi:10.1083/jcb.200806030

Vicente-Manzanares, M., Newell-Litwa, K., Bachir, A. I., Whitmore, L. A. and Horwitz, A. R. (2011). Myosin IIA/IIB restrict adhesive and protrusive signaling to generate front-back polarity in migrating cells. *J. Cell Biol.* **193**, 381-396. doi:10.1083/jcb.201012159

Waters, J. C. and Wittmann, T. (2014). Quantitative imaging in cell biology. Preface. *Methods Cell Biol.* **123**, xix-xxx. doi:10.1016/B978-0-12-420138-5.09983-3

Webb, D. J., Parsons, J. T. and Horwitz, A. F. (2002). Adhesion assembly, disassembly and turnover in migrating cells – over and over and over again. *Nat. Cell Biol.* **4**, E97-E100. doi:10.1038/ncb0402-e97

Webb, D. J., Donais, K., Whitmore, L. A., Thomas, S. M., Turner, C. E., Parsons, J. T. and Horwitz, A. F. (2004). FAK-Src signalling through paxillin, ERK and MLCK regulates adhesion disassembly. *Nat. Cell Biol.* **6**, 154-161. doi:10.1038/ncb1094

Wilson, C. A., Tsuchida, M. A., Allen, G. M., Barnhart, E. L., Applegate, K. T., Yam, P. T., Ji, L., Keren, K., Danuser, G. and Theriot, J. A. (2010). Myosin II contributes to cell-scale actin network treadmilling through network disassembly. *Nature* **465**, 373-377. doi:10.1038/nature08994

Worthylake, R. A., Lemoine, S., Watson, J. M. and Burridge, K. (2001). RhoA is required for monocyte tail retraction during transendothelial migration. *J. Cell Biol.* **154**, 147-160. doi:10.1083/jcb.200103048

Yasuda-Yamahara, M., Rogg, M., Frimmel, J., Trachte, P., Helmstaedter, M., Schroder, P., Schiffer, M., Schell, C. and Huber, T. B. (2018). FERMT2 links cortical actin structures, plasma membrane tension and focal adhesion function to stabilize podocyte morphology. *Matrix Biol.* **68-69**, 263-279. doi:10.1016/j.matbio.2018.01.003

Zenke, F. T., Krendel, M., Dermardirossian, C., King, C. C., Bohl, B. P. and Bokoch, G. M. (2004). p21-activated kinase 1 phosphorylates and regulates 14-3-3 binding to GEF-H1, a microtubule-localized Rho exchange factor. *J. Biol. Chem.* **279**, 18392-18400. doi:10.1074/jbc.M400084200

Zhang, Z., Mu, Y., Veevers, J., Peter, A. K., Manso, A. M., Bradford, W. H., Dalton, N. D., Peterson, K. L., Knowlton, K. U., Ross, R. S. et al. (2016). Postnatal loss of Kindlin-2 leads to progressive heart failure. *Circ. Heart Fail.* **9**, e003129. doi:10.1161/CIRCHEARTFAILURE.116.003129